Osaka University Knowledge Archive

Title	Ion-Beam Lithography for Fabricating Devices with Nanometer Structures
Author(s)	森脇, 和幸
Citation	大阪大学, 1982, 博士論文
Version Type	VoR
URL	https://hdl.handle.net/11094/1480
rights	
Note	

Osaka University Knowledge Archive : OUKA

https://ir.library.osaka-u.ac.jp/

Osaka University

Ion-Beam Lithography for Fabricating Devices with Nanometer Structures

Kazuyuki Moriwaki

Faculty of Engineering Science
Osaka University, Toyonaka, Osaka, Japan

February 1982

Contents

1. Introduction - 1

References - 5

2. Ion-Beam Exposure of Resists (IBER)

2-1. Introduction - 6

2-2. Experimental Procedure - 8

2-3. Exposure Characteristics of PMMA Resist

2-3-1. Introduction - 12

2-3-2. Developed Depth - 13

2-3-3. Deposited Energy Distribution - 17

2-4. Pattern Replication in PMMA resist with Au mask

2-4-1. Introduction - 26

2-4-2. Fabrication of Au mask - 27

2-4-3. Replication of Au Mask-Pattern - 33

2-5. Exposure Characteristics of FPM and AZ1350 Resists

2-5-1. Introduction - 37

2-5-2. FPM Resist - 37

2-5-3. AZ1350 Resist - 43

2-6. Statistical Problems of Impinging Ions - 47

2-7. Conclusions - 49

References - 51

3. Ion-Bombardment-Enhanced Chemical-Etching (IBECE)

3-1. Introduction - 54

3-2. Experimental Procedure - 55

3-3. IBECE characteristics of Si - 57

3-4. Pattern Profile of Si

3-4-1. Introduction - 63

3-4-2. Calculation of Etched Profile - 64

3-4-3. Observed Etched Profile - 67

3-4-4. Optimum Condition - 72

3-4-5. Fabrication of Submicron Pattern - 76

3-5. IBECE Characteristics of SiO - 79

3-6. Conclusions - 81

References - 83

4. Application of Au Free-Standing Mask to X-Ray Transmission-Grating

4-1. Introduction - 85

4-2. Calculation of Diffraction Efficiency - 85

4-3. Fabrication of Au Transmission-Grating - 89

4-4. Conclusions - 92

References - 92

5. Conclusions - 93

Acknowledgements - 95

1. Introduction

Microfabrication has been making remarkable progress with the growth of Si LSI (Large Scale Integrated Circuit) technology.[1] Currently, Microfabrication is a cornerstone to develop higher performance devices not only of Si LSI having higher packing density and higher operating speed, but also of GaAs IC, superconducting devices, optical IC, surface acoustic devices and so on, for various fields of electronics particularly for computer or communication.

As the man-made feature-size is decreasing to less than 10 nm[2-5] which is nearing lattice constant of solids, new high speed devices have been proposed utilizing the small size. One of the interesting new device is the ballistic electron device[6] using the ballistic motion of electron in a shorter path than the electron mean-free-path in a semiconductor. Another important example of the new devices is based on the quantum size effect in a semiconductor.[7] Though these future devices have attractive features, the feasibility depends on the progress of microfabrication.

Looking back the trends of micriofabrication to reduce the feature size, some breakthroughs existed. Optical lithography[1] has been a main and powerful tool in microfabricaiton technology because of its simplicity and its high productivity. Due to diffraction effect, however, 1 μm is the practical limit of optical lithography. New approaches to break the micron limit is

called submicron lithography which includes electron-beam lithography, ion-beam lithography, deep UV lithoraphy, x-ray lithography and various ion etching techniques, which are summarized in Fig. 1-1. Electron-beam lithography has now become the most important tool for the submicron lithograpy, as it can generate arbitrary patterns and it has inherently high resolution as small as 10 nm.[2,5] But electron scattering effect both in the resist and in the substrate severely limits the minimization of the pattern to about 0.2 μm with a practical electron-beam-lithography system.[8] An excellent way to reduce the scattering effect is to adopt a thin substrate with less than 100 nm thickness,[9] thin resist and higher electron energy than 20 keV.[9,10] But as it is rather a sophisticated technique to use a thin substrate, it is difficult to be applied to all fields of submicron lithography. Though electron beam lithography system with high elecron energy of 30-50 keV is useful,[10] it can not overcome the scattering effect completely.

Recently, an interest for focused-type scanning ion-beam lithography has been stimulated by researches on high intensity scanning ion-probe[11] and ion-beam exposure of resist materials.[12] Ion-beam lithography is expected to exhibit high resolution with less than 100 nm which is a practical limit with a conventional electron-beam-lithography system. The high resolution of ion-beam lithography can be inferred from small lateral range of the incident ions and secondary electrons. But detailed research on ion-beam lithography has not been performed and is strongly desired now.

It should be pointed out that utility of ion beam as a tool for lithography is not only the high resolution but its wide applicability to direct engraving or doping processes without intermediate masking processes[13] as well as to the exposure of resists. For the above mentioned reason, ion-bombardment-enhanced chemical-etching is a promising technique as direct etching process with submicron resolution.

In the present study, researches on ion-beam lithography including ion-beam exposure of resists and ion-bombardment-enhanced chemical-etching have been performed to confirm its utility for nanometer lithography.

Chapter 2 describes characteristics of proton-beam exposed PMMA, FPM and AZ1350 resists with a conventional ion implanter. The deposited energy distribution in a resist and the developed profile of a resist is studied in detail for PMMA as a standard resist. The resolution is investigated by replicating Au free-standing mask-patterns to the resists.

Chapter 3 treats the ion-bombardment-enhanced chemical-etching of Si and SiO_2 with a conventional ion implanter. The etched profile of Si is investigated in detail with an accuracy of 10 nm.

Chapter 4 is on an application of the Au free-standing mask to a diffraction grating for x-ray spectroscopy. Fabrication of successful Au transmission-gratings and calculation of the diffraction efficiency are described.

Chapter 5 summarizes the conclusions of the present study.

Throughout the present thesis, the following abbreviations are used. That is Ion-Beam Lithography (IBL), Electron-Beam Lithography (EBL), Ion-Beam Exposure of Resists (IBER) and Ion-Bombardment-Enhanced Chemical-Etching (IBECE).

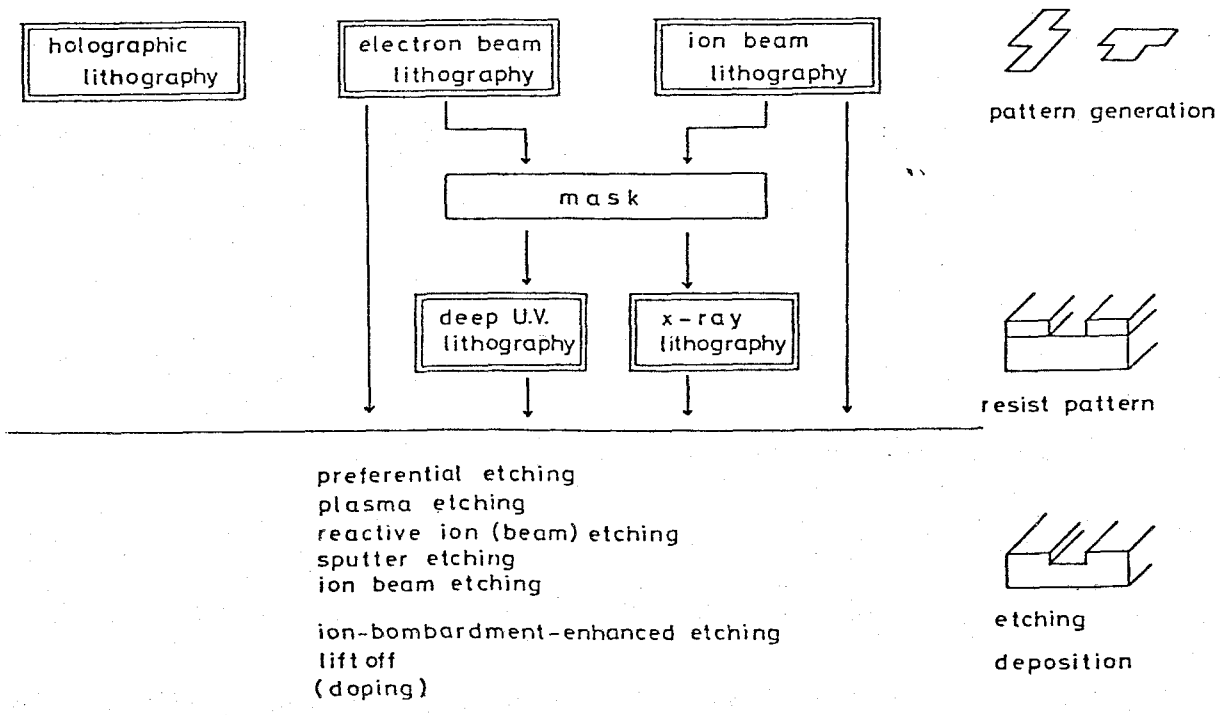

Fig. 1-1. Microfabrication processes with submicron resolution.

References

1) N.G.Einspruch: VLSI Electronics -Microstructure Science- (Academic Press, New York, 1981) Vol.1, Vol.2.

2) A.N.Broers, W.W.Molzen, J.J.Cuomo and N.D.Wittels: Appl. Phys. Lett. 29 (1976) 596.

3) D.C.Flanders; J. Vac. Sci. Technol. 16 (1979) 1615.

4) S.P.Beaumont, P.G.Bower, T.Tamamura and C.D.W.Wilkinson: Appl. Phys. Lett. 38 (1981) 436.

5) M.Issacson and A.Murray: J. Vac. Sci. Technol. 19 (1981) 1117.

6) M.S.Shur and L.F.Eastman: Solod-State electron. 24 (1981) 11.

7) H.Sakaki: Jpn. J. Appl. Phys. 19 (1980) L735.

8) G.R.Brewer: Electron-Beam Technology in Microelectronic Farication (Academic Press, New York, 1977).

9) A.N.Broers, J.M.E.Harper and W.W.Molzen; Appl. Phys. Lett. 35 (1978) 392.

10) T.R.Neill and C.J.Bull: Electron. Lett. 16 (1980) 621.

11) R.L.Seliger, T.W.Ward, V.Wang and R.L.Kubena: Appl. Phys. Lett. 34 (1979) 310.

12) M.Komuro, N.Atoda and H.Kawakatsu: J. Electrochem. Soc. 126 (1979) 483.

13) R.L.Kubena, C.L.Anderson, R.L.Seliger, R.A.Jullens and E.H.Stevens: IEEE Electron Devices Lett. EDL-2 (1981) 152.

2. Ion Beam Exposure of Resist (IBER)

2-1. Introduction

IBL is a technique similar to EBL as illustrated in Fig. 2-1, only substituting ion beam for electron beam in principle. But the substitution provides the excellent high-resolution feature of IBL, because the lateral spread of deposited energy in a resist is negligibly small compared with that of EBL due to small lateral spread of ions and small range of secondary electrons ejected from the substrate atoms, as illustrated in Fig. 2-2. Currently, researches both on ion-beam exposed resists[1-12] and on scanning IBL system[13-18] have been independently investigated.

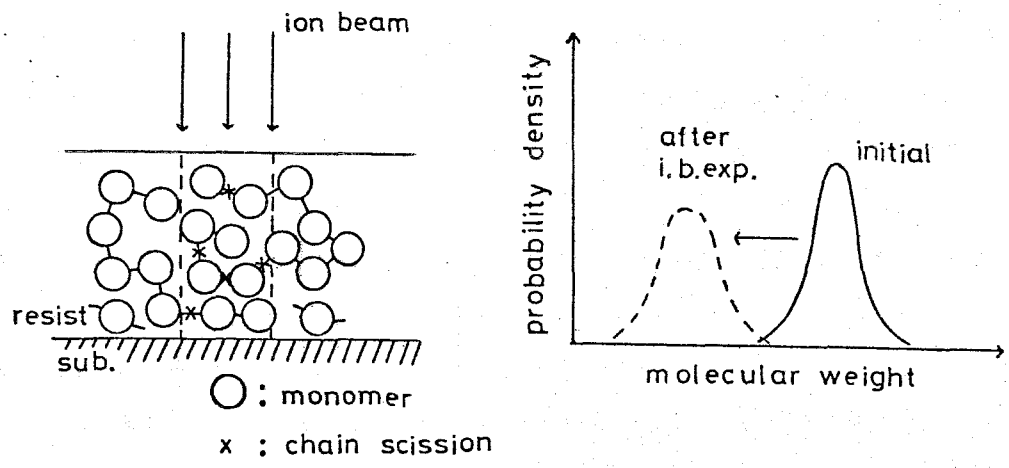

Fig. 2-1. Illustration of the mechanism to obtain a pattern in a positive resist by IBER.

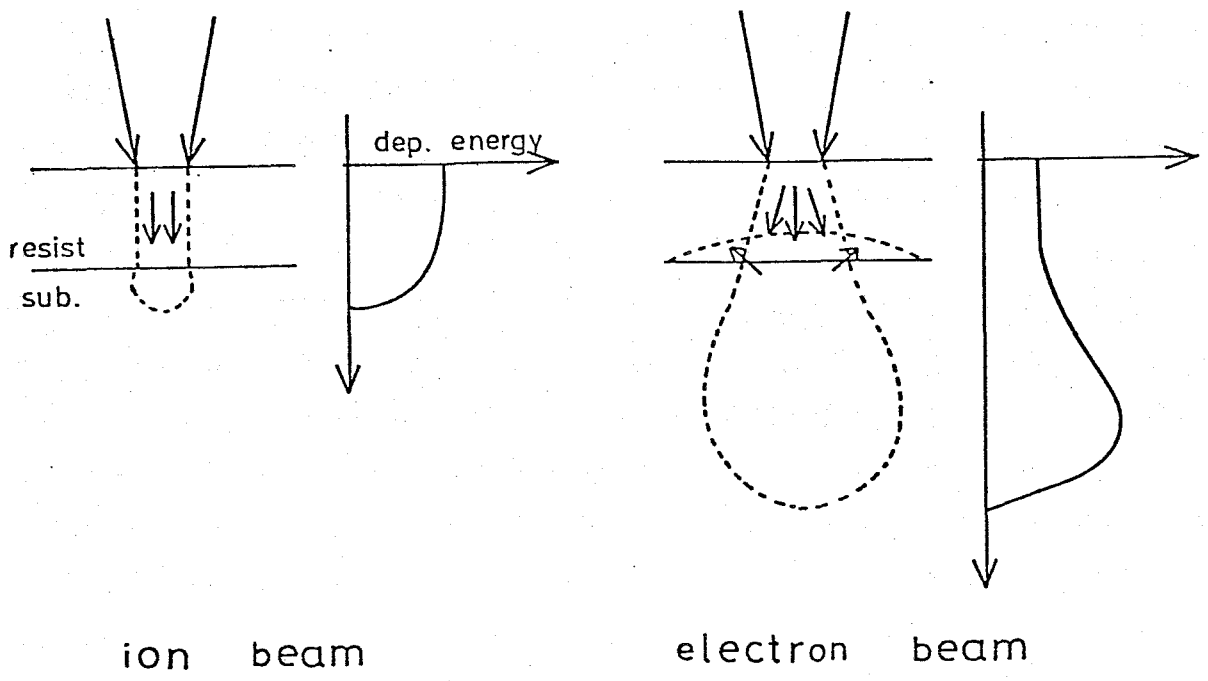

Fig. 2-2. Schematic comparison of IBER with EBL. The deposited energy contour is shown by a dotted curve.

The current problems for IBER are summarized as followed.

(i) To develop a reliable system for scanning focused IBL.

(ii) To study the exposure characteristics of resists and optimum conditions for pattern fabrication.

(iii) To determine the ion distribution in a resist due to the ion scattering effect, in order to investigate the pattern profile and the resolution.

(iv) To investigate the damage in a substrate induced by the ion bombardment.

In the present study, the problems (ii) and (iii) have been taken to be solved using proton as the exposing ion and PMMA (poly methyl methacrylate), FPM (poly tetrafluoropropyl methacrylate)[19] and AZ1350 as ion-beam resists.

The reason to select proton as the exposing ion is that the ion range is relatively deep to obtain high aspect-ratio patterns at a moderate ion energy, and that analysis of the deposited energy distribution in a resist is simple and hence understanding of essence of IBER is easier, as is dicussed in section 2-3-3.

In the following section of this chapter, PMMA has been used mainly as a standard resist to study IBER in detail, regarding the deposited energy in the resist (in section 2-3), and the replicated pattern and the resolution with Au mask (in section 2-4). The exposure characteristics of FPM and AZ1350 resists are described in section 2-5. Section 2-6 studies statistical problems of the impinging ions.

2-2. Experimental Procedure

A conventional ion-implanter as shown in Fig. 2-3. was used to expose resists with 50 keV proton beam. The ion-beam exposing conditions are summarized in Table 2-1. Resists were spin-coated on a Si wafer, and baked before the ion bombardment. The thickness of the resist film was 0.34-0.45 μm for pattern fabrication and about 1 μm for measurements of the exposed

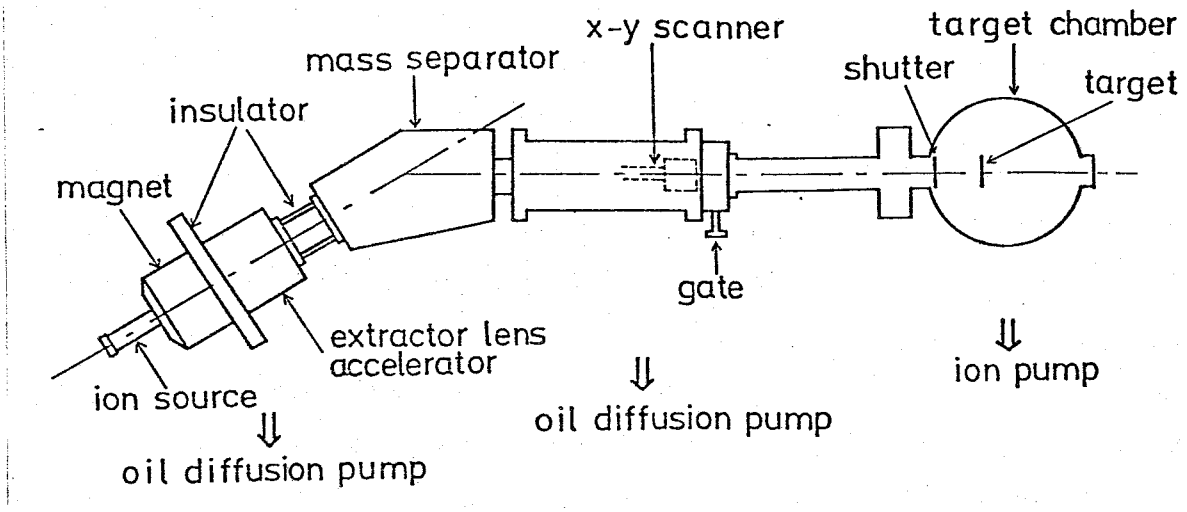

Fig. 2 3. Schematic diagram of ion implanter.

Table 2-1. Ion-beam exposure conditions with an ion implanter.

ION	H^+
ACC. VOL.	50 kV
DOSE	8×10^{-8} - 5×10^{-6} C/cm^2
DOSE RATE	3 - 14 nA/cm^2
RESIST	PMMA, FPM, AZ1350

thickness. Prebaking conditions of resists were 170° C, 110 min for PMMA, 170° C, 30 min for FPM and 90° C, 10 min for AZ1350. The resisit after proton beam irradiation were developed by a mixed solution of MIBK and IPA at a temperature of 23-25°C for PMMA and FPM, and by the AZ1350 developer for AZ1350. Developed thickness of the resist was measured with a interference microscope. Comparison of IBER with IBL was performed with a EBL system (JEOL JBX-5B) as the block diagram is shown in Fig. 2-4.

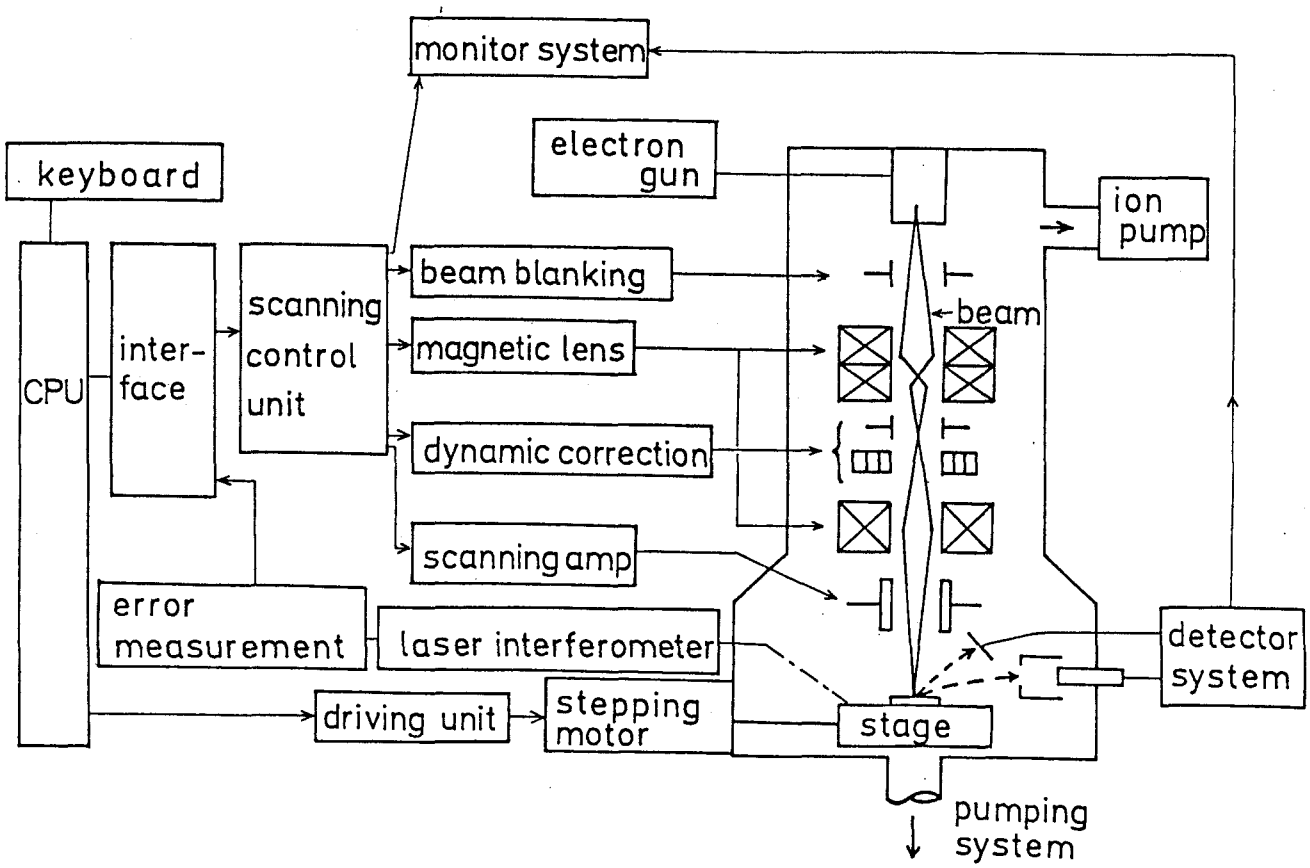

Fig. 2-4. Block diagram of electron beam exposure system.

Sensitivity and γ-value[20] were determined by a exposure curve of resist, as defined in Fig. 2-5. The fabricated patterns were observed with a scanning electron microscope (JEOL JSM35) whose resolution is 7 nm.

Au masks were fabricated with the EBL system (JEOL JBX-5B) and an ion-beam etching system (Elionics ISM-S) as shown in Fig. 2-6.

The operation of the EBL system is based on the vector scanning with a round spot of 50 nm diameter. A accelerating voltage and a typical current of the electron beam are 20 kV and 0.01 - 5 nA, respectively.

The ion-beam etching system was operarted with a accelerating voltage of 500 V and an ion-beam current of 0.2 - 0.4 mA/cm^2 .

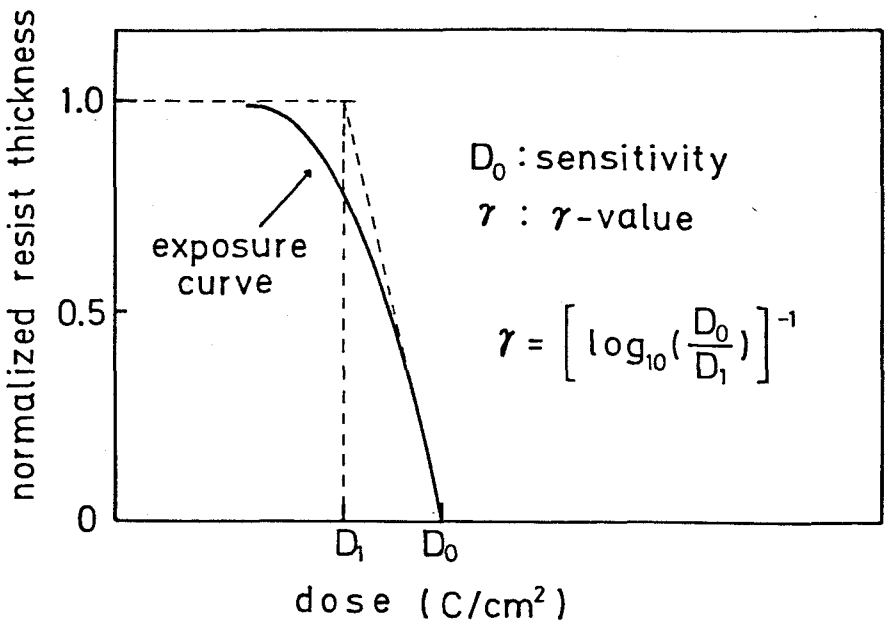

Fig. 2-5. Definition of sensitivity and γ-value for a positive resist.

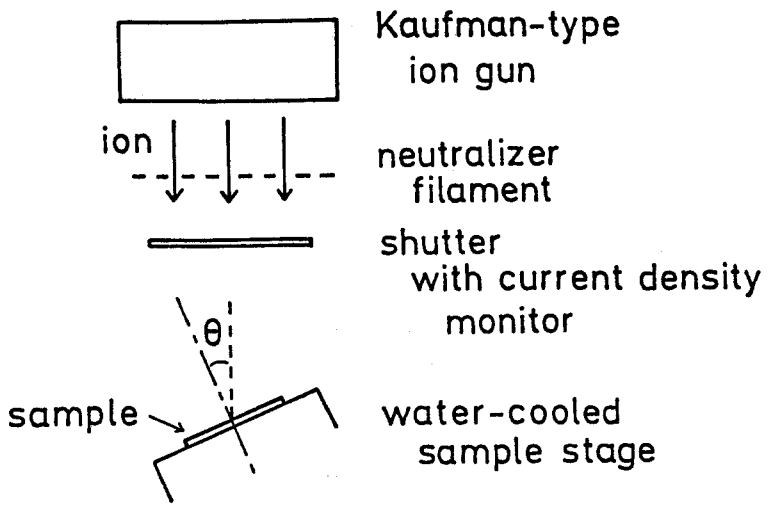

Fig. 2-6. Schematic diagam of ion-beam etching apparatus.

2-3. Exposure Characteristics of PMMA Resist

2-3-1. Introduction

In this section, exposure characteristics of PMMA are shown, including the sensitivity and the γ-value. And the deposited energy distribution in PMMA resist is calculated to compare with measured developed depth as a function of developing time.

2-3-2. Developed Depth

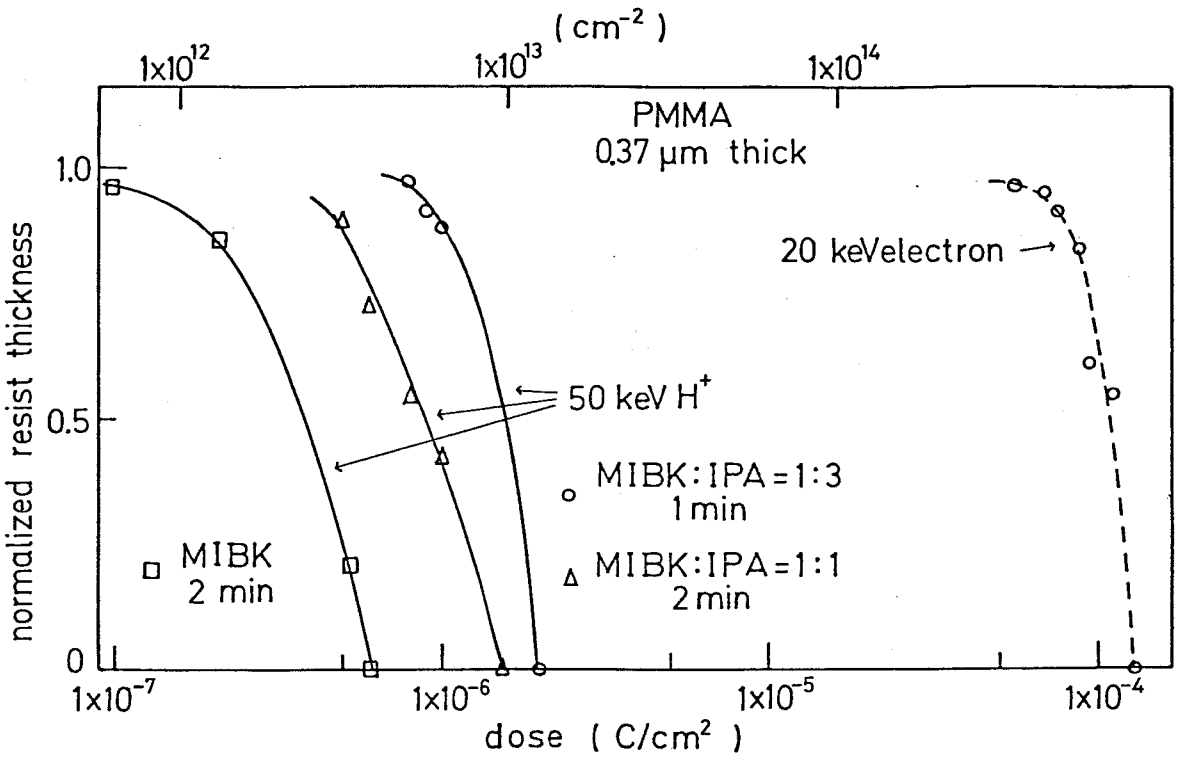

Fig. 2-7. Exposure characteristics of PMMA resist by 50 keV proton beam for some developing conditions together with that by 20 keV electron beam.

Figure 2-7 shows the exposure characteristics of PMMA by 50 keV proton beam for three kinds of developer together with that by 20 keV electron beam. It can be seen that sensitivity of PMMA

resist is $2x10^{-6}$ C/cm^2 and is 70 times higher for 50 keV proton beam than that for 20 keV electron beam for a developing condition of MIBK:IPA = 1:3.

It should be noted that the sensitivity defined as that in Fig. 2-4 is not inherent one to the resist itself and changes by altering the ion-beam conditions such as kind of ion or ion energy which have no relation to the resist itself. The sensitivity is a practically important parameter which is a minimum dose required for full development of the resist down to the substrate surface. So the high sensitivity should be considered low ion-dose for fabricating pattens.

The higher sensitivity by about two order of magnitude for IBER than for EBL is understandable from the difference of the deposited energy density in a resist.[2] This is inferred from the fact that the ion range is shorter than the electron range by about two order of magnitude for the condition in Fig. 2-5, as illustrated in Fig. 2-2. Currently conventional EBL systems adopt the electron energy of 20 keV. Although lower energy of electron beam than 20 keV makes the sensitivity higher for the electron beam, lateral spread of energy density deposited in a resist becomes too large to fabricate submicron patterns because of the electron scattering effect.[20] It can be concluded that IBER is a very effective means to obtain fine patterns in a resist because confinement of the incident ions in an irradiated part of a resist is good both in the lateral and the depth direction, and almost all the initial ion-energy is consumed in the resist to exposed the resist.

The γ-value (as defined in Fig. 2-4) corresponding to the slope of the characteristic curve in Fig. 2-5 is 3.3 for a developer of MIBK:IPA = 1:3, and 3.0 for that of both MIBK:IPA = 1:1 and MIBK, and is not so low as 4.7 for 20 keV electron beam. The -value influences accuracy of the replicated patterns after development. The γ-value for IBER in Fig. 2-5 is relatively high to achieve submicron patterns considering the case for EBL.[20]

Developed thickness of PMMA as a function of developing

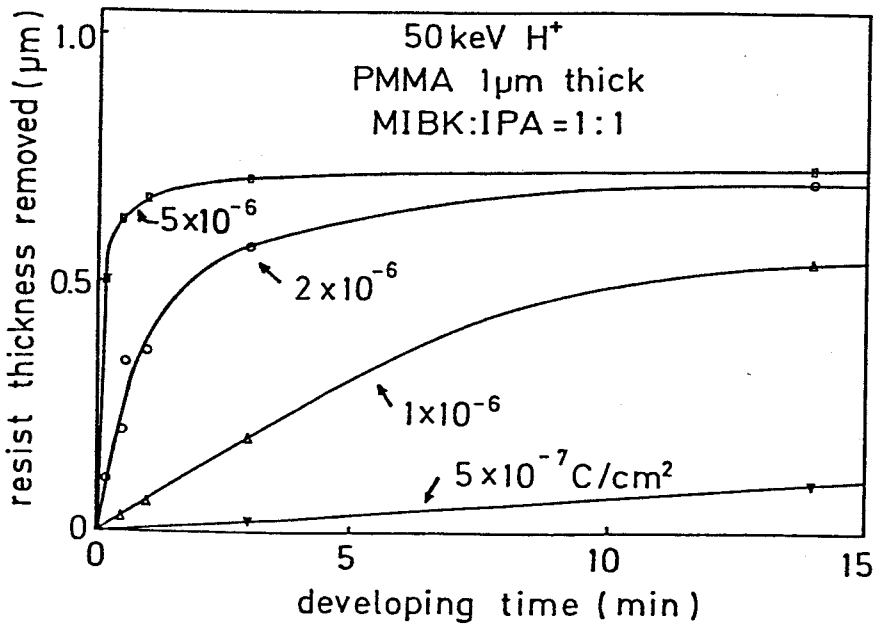

Fig. 2-8. PMMA resist thickness removed vs. developing time after irradiation of 50 keV proton beam for a developer of MIBK:IPA = 1:1.

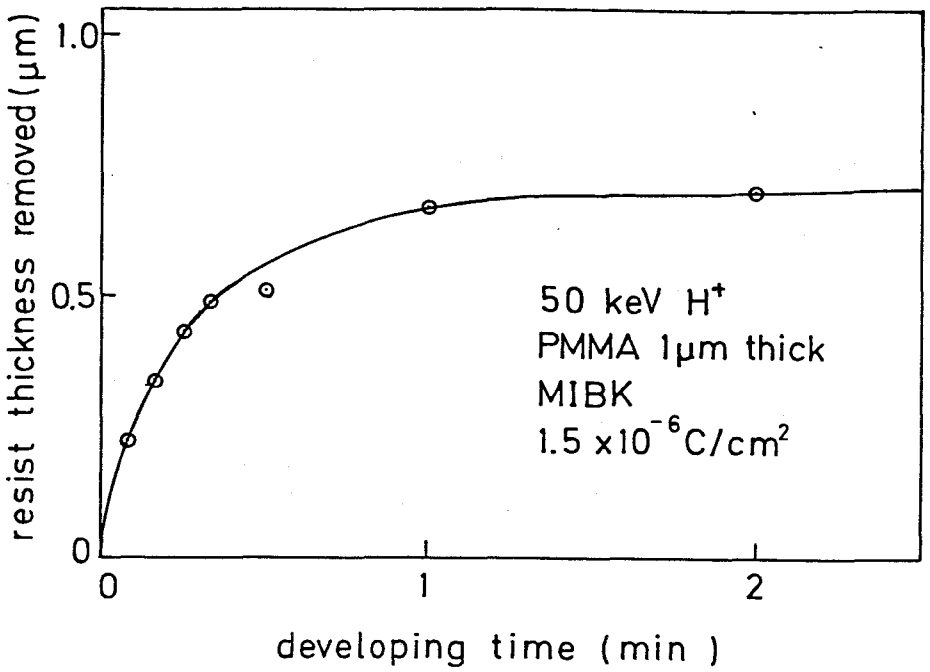

Fig. 2-9. PMMA resist thickness removed vs. developing time after irradiation of 50 keV proton beam for a developer of MIBK.

time after proton-beam irradiation is shown using a developer of MIBK:IPA = 1:1 in Fig. 2-8 and using a developer of MIBK in Fig. 2-9. The developed thickness saturates after an developing time long enough. Because the initial thickness of PMMA is 1 μm and is sufficiently thick to stop almost all ions in the resist. It can be seen from Fig. 2-8 and 2-9 that 0.7 μm-deep patterns can be fabricated in PMMA resist with 50 keV proton beam. The ion range and characteristics of the proton-beam exposed PMMA are considered in detail in section 2-3-3 using Fig. 2-8.

2-3-3. Deposited Energy Distribution

The etched profile in a resist by IBER is important for its applications to devices. What defines the etched profile is a latent image of the deposited energy in a resist exposed by ion-beam and dissolution characteristics of the resist for the developer used.

Dissolution characteristics of resists[21-25] have been investigated for electron-beam exposure together with the deposited energy distribution.[26] Particularly, Monte Carlo simulation[27-31] of the deposited energy distribution for EBL was successfully adopted to simulate the observed undercutting profile in a resist[20] due to the electron scattering effect both in the resist and in the substrate. Monte Carlo simulation[32] have been applied to the proximity-effect correction[33] which is inevitable for EBL in VLSI production.

As for IBER, however, reliable theory has not been established to calculate the ion range or the deposited energy distribution for both a light ion such as proton and a light-mass target such as polymer resist, because of few experiments to be compared. Though preliminary calculations have been carried out for the deposited energy distribution in a resist exposed by ion beam,[2,4] thorough comparison between the calculations and the experiments is required for IBER.

In this section, A new simple approach with holding sufficient accuracy is proposed in order to calculate one dimensional distribution of the deposited energy in depth

direction.[34] Comparison of the calculated distribution with experiments for PMMA is also presented using dissolution characteristics of PMMA.

The energy loss process of incident ions in a resist is devided into two components of electronic and nuclear collision,[35] while only electronic energy loss is to be considered in EBL.[20] But, for light ion such as proton, electronic excitation is the dominant energy loss process, though the nuclear collision cannot be neglected completely around the ion path where the ion has too low energy to penetrate further.[2,4] In the present calculation, the energy loss by nuclear collision has been neglected.

Stopping power S(E) for an ion possessing energy E which depends on depth z is defined as

$$\frac{\partial E(z,r)}{\partial z} = -S(E(z,r)), \qquad (2\text{-}1)$$

where r is a depth at which the ion stop to penetrate. The number of ion N(r) in the resist is approximately given by Gaussian distribution as

$$N(r) = \frac{D}{\sqrt{2\pi}\Delta R}\cdot\exp[-\frac{1}{2}\cdot(\frac{r-R}{\Delta R})^2], \qquad (2\text{-}2)$$

where D is ion dose and R and ΔR are parameters of the average projected ion range and the standard deviation of the projected ion range, respectively. The values of R and ΔR are assumed to be given in the present analysis, and are to be verified by

comparing the calculated results with experiments.

Usual meaning of the stopping power is average stopping power for many ions penetrating down to various depthes and feeling various stopping power. In the present analysis, for an ion, a stopping power S(E) through which the ion losees the possessing energy is assumed to be given by proportionate to the average stopping power $\tilde{S}(E)$ as

$$S(E) = k \cdot \tilde{S}(E), \tag{2-3}$$

where k is constant for all E but depends on r.

Total ion range is given by integration of 1/S(E) as is derived from eq. (2-1). As the total range is nearly equal to projected ion range for proton with an ion energy of around 50 keV,[4] r is calculated by integrating eq. (2-1). Boundary conditions for ion energy E are given by

$$E(0,r) = E_0, \tag{2-4}$$

$$E(r,r) = \varepsilon, \tag{2-5}$$

where ε is to be zero theoretically but is taken to be 1 keV in the following calculation because the available stopping power at such a low ion energy is not reliable and the resultant ion range would not change practically by the neglect of the lower energy ion.

Using eqs. (2-4), (2-5), integration of eq. (2-1) from ε to

E yields

$$[\ 1 - (z/r)\ ] = \frac{1}{R_t} \cdot \int_{\varepsilon}^{E} \frac{dE}{\tilde{S}(E)}\ , \qquad (2\text{-}6)$$

where R_t is total ion range calculated from the average stopping power as

$$R_t = \int_{\varepsilon}^{E_0} \frac{dE}{\tilde{S}(E)}\ , \qquad (2\text{-}7)$$

and k as defined in eq. (2-3) is represented by R_t as

$$k = R_t/r. \qquad (2\text{-}8)$$

Ion energy E(z,r) at a depth z can be calculated by the eq. (2-6). Hence deposited energy distribution P(z) in the resist is calculated by integrating S(E(z,r)) using the weight function of N(r) in eq. (2-2),

$$P(z) = \int_0^{\infty} S(E(z,r))\cdot N(r)\ dr$$

$$= \int_0^{\infty} (R_t/r)\cdot \tilde{S}(E(z,r))\ dr. \qquad (2\text{-}9)$$

In the following part of this section, the deposited energy distribution in PMMA resist exposed by 50 keV proton-beam is calculated by using above mentioned equations.

Fig. 2-10 shows the calculated stopping power $\tilde{S}(E)$ by interpolation of data[36] using average atomic number of 3.6 for

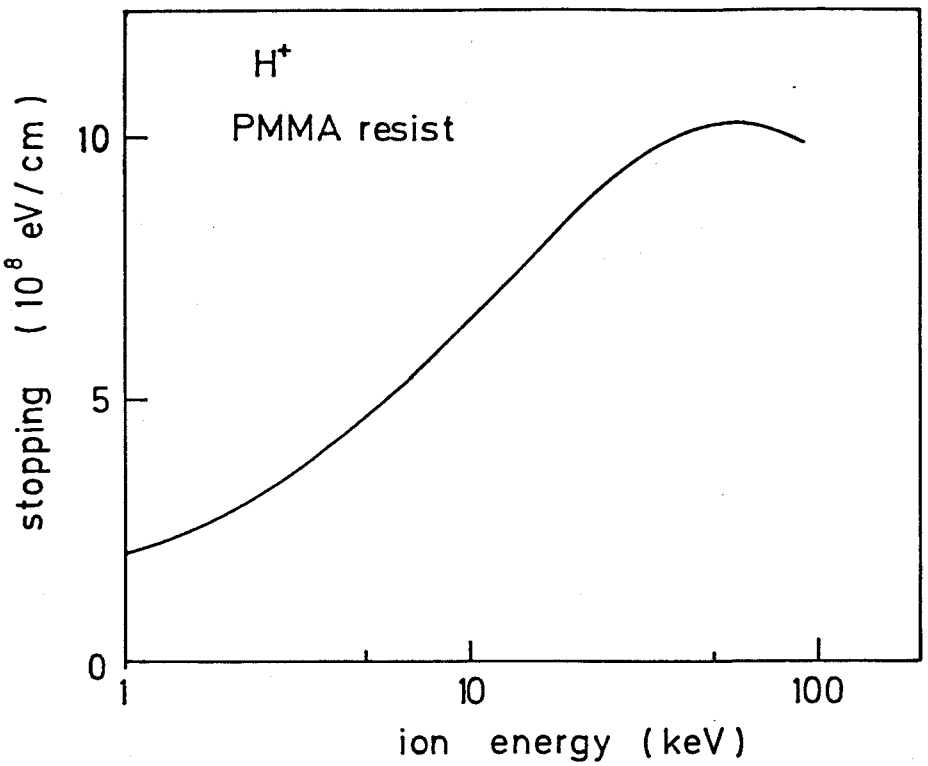

Fig. 2-10. Calculated electronic stopping power for proton beam in PMMA resist.

PMMA. Using the $\tilde{S}(E)$ and eq. (2-7), R_t was calculated to be 653 nm. Ion energy E(z,r) is calculated numerically using eq. (2-6) as shown in Fig. 2-11, where the depth z is normalized by the R_t. The resultant distribution of the deposited energy P(z) are shown in Fig. 2-12, calculated from eq. (2-9) for some ion doses using R of 650 nm and ΔR of 30 nm.

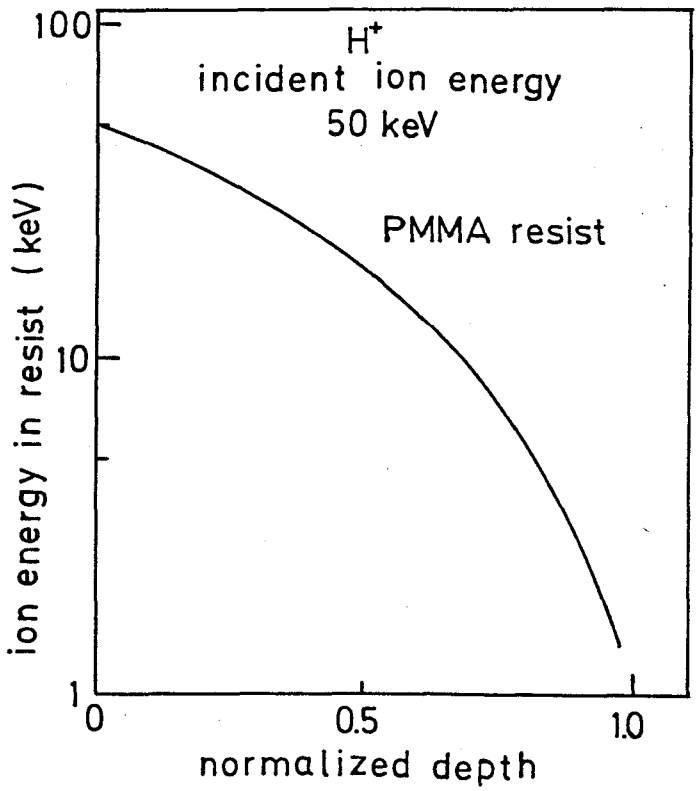

Fig. 2-11. Calculated Energy of proton penetrating in PMMA resist with an initial energy of 50 keV.

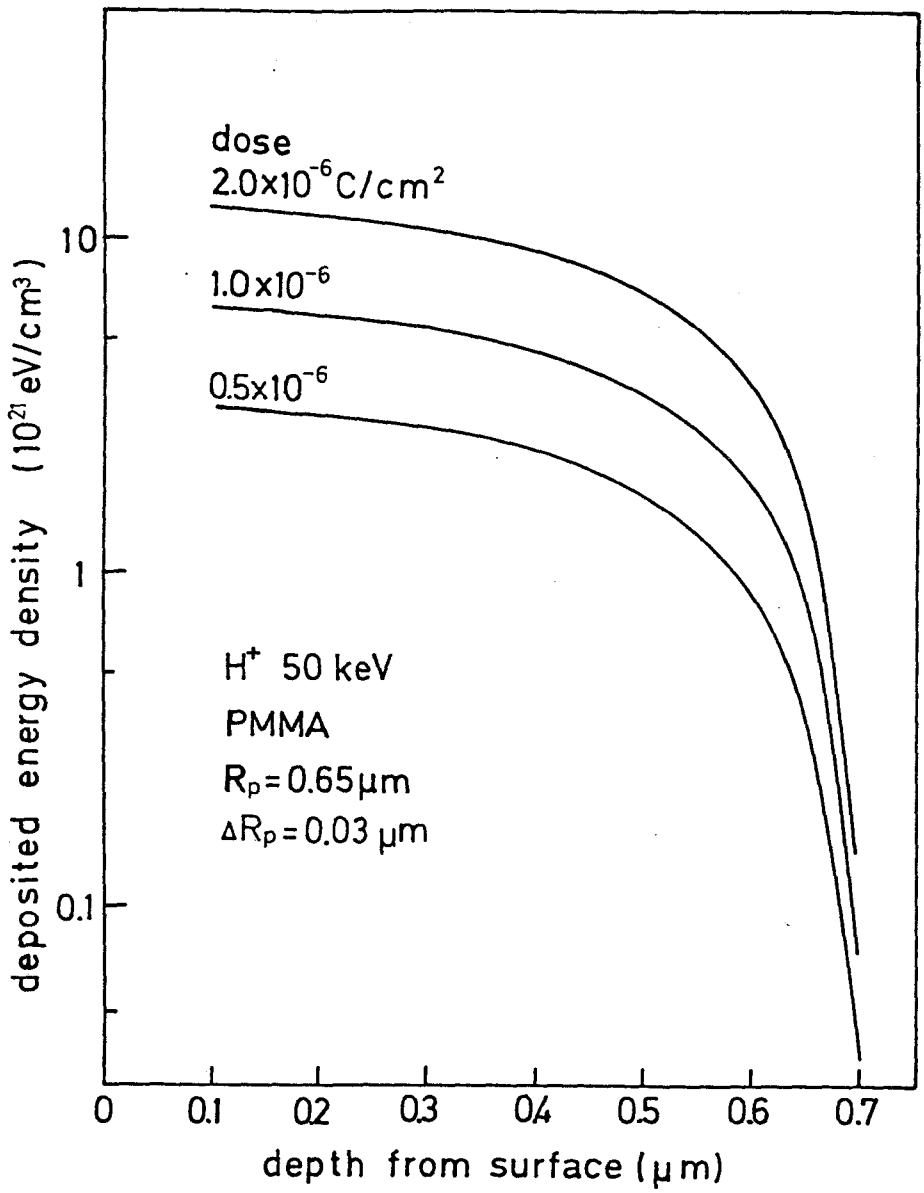

Fig. 2-12. Calculated distribution of deposited energy density in PMMA resist.

Verification of the present analysis of deposited energy distribution is carried out by comparing the experiment shown in Fig. 2-8, using dissolution characteristics of PMMA.[2,22] Dissolution rate V of a resist is represented as[22]

$$V = V_0 + B\left(\frac{1}{M_n} + \frac{S_e \cdot G_e}{\rho \cdot N_A \cdot 100}\right)^A, \qquad (2\text{-}10)$$

where V_0 : dissolution rate for the unexposed resist,

M_n : initial number-average molecular weight,

S_e : electronic stopping power,

G_e : G-value for chain scission of the resist caused by electronic excitation,

ρ : density of the resist

N_A : Avogadro's number.

And the values of A and B are tobe determined experimentary.

Using parameters ρ = 1.2 g/cm , M_n = 125000, G_e = 1.7,[2] and V_0 = 0, and using S_e in Fig. 2-12, the dissolution rate in Fig. 2-8 is accurately predicted as shown in Fig. 2-13, where parameters of A and B were found to be 2.8 and 5.0×10^{10} nm/sec. The agreement of the calculation and the experiment in Fig. 2-13 is good with an accuracy less than 30 nm, which verifies that the present calculation is very useful method in spite of its simple treatment. Moreover, the ion range and the standard deviation of ion range of 650 nm and 30 nm, respectively, assumed in the present calculation are shown to be accurate values.

The electronic stopping power is approximately proportionate to square root of ion energy.[36] If so, total ion range is

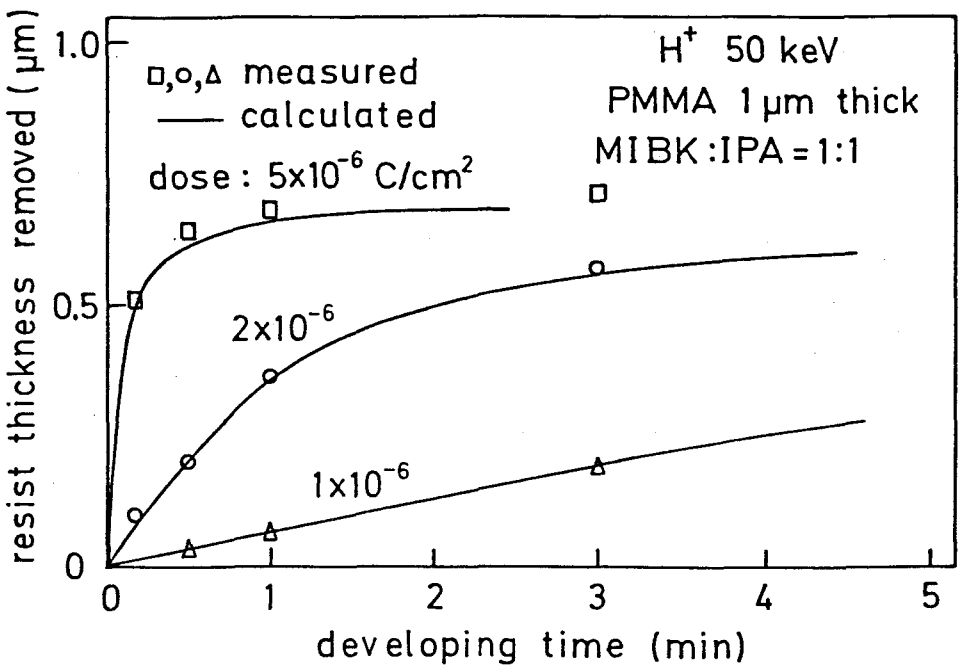

Fig. 2-13. Comparison of calculated developed depth with experiment.

shown to be proportionate to square root of ion energy solving eq. (2-7), which is nearly equal to the developed depth after the saturation as can be seen in Fig. 2-13. The square root dependance of ion range on the proton energy are confirmed in Fig. 2-14.

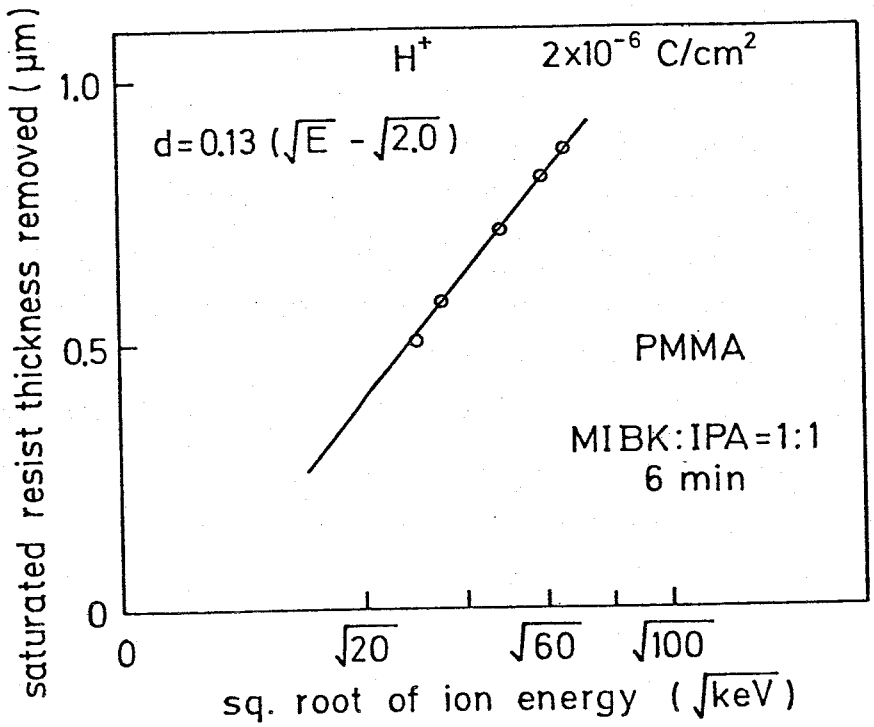

Fig. 2-14. Saturated etched depth d of PMMA as a function of ion energy E.

2-4. Pattern Replication in PMMA resist with Au Mask

2-4-1. Introduction

In this section, resolution of IBER has been investigated by replicating Au free-standing mask in PMMA resist.[8] Some masks

for ion beam replication have been proposed using Al_2O_3 ,[5] Si film[7] and polyimide membrane[12] as the supporting material under the mask patterns. But ion scattering effect in the supporting film limits their applicability. For simple patterns such as line patterns or grating patterns, the Au free-standing mask is useful to investigate replicated pattern profiles as well as to utilize the replicated patterns, though arbirtrary patterns cannot be fabricated. The fabrication process for the Au free-standing mask is described in 2-4-2. And the replication of the mask to PMMA resist is presented in 2-4-3.

2-4-2. Fabrication of Au mask

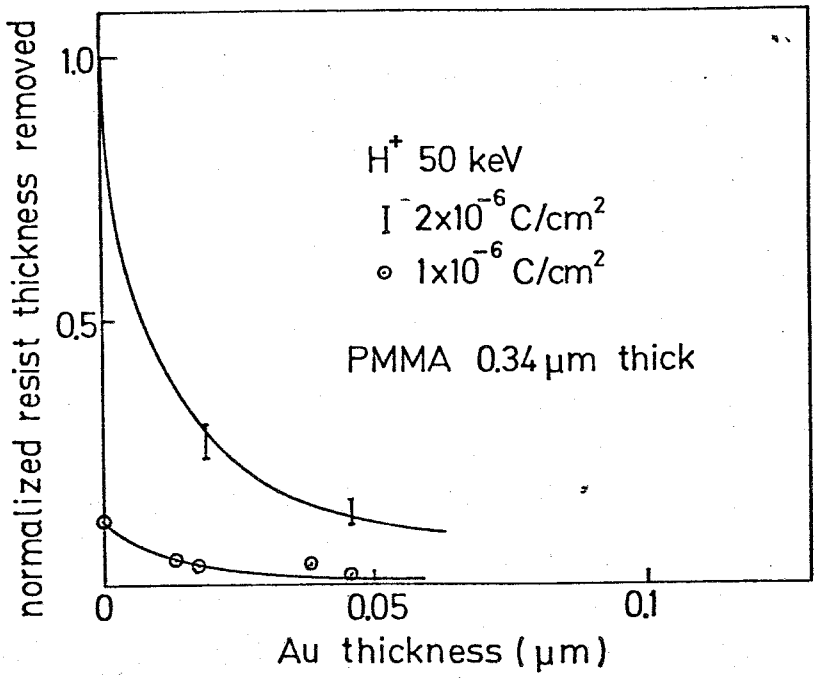

Fig. 2-15. Developed depth of PMMA after proton beam irradiation through Au film.

Au is suitable mask material to stop ions because of its high mass number and its ease for fabrication processes. Exposure characteristics of PMMA under Au film was measured to determine the necessary thickness of the Au mask to be able to form patterns as shown in Fig. 2-15. It can be seen that with an ion dose of $2x10^{-6}$ C/cm^2, the developed thickness decreased to 1/10 of the initial thickness of PMMA, if the Au film of 50 nm thickness exist on the PMMA. From Fig. 2-15, the very thin

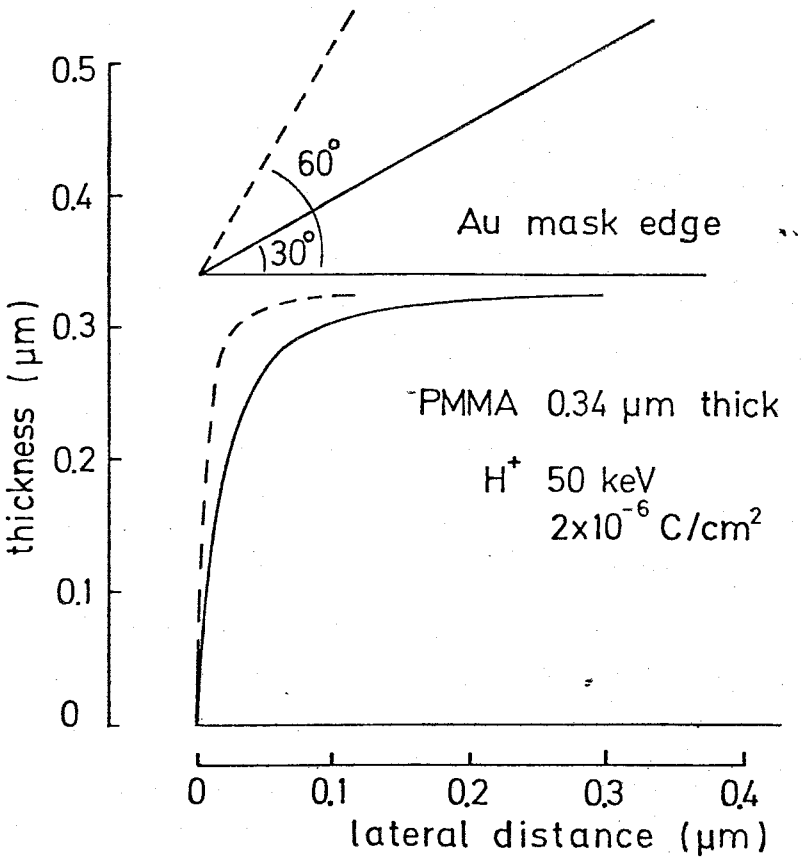

Fig. 2-16. Pattern profile of PMMA under Au mask edge.

Au-film thicker than 50 nm can be inferred to make a high contrast patterns in PMMA. Fig. 2-16 shows pattern profile of PMMA under Au mask edge estimated from the characteristics in Fig. 2-15. Under even an edge-angle of 30°, steep edge of PMMA pattern can be obtained.

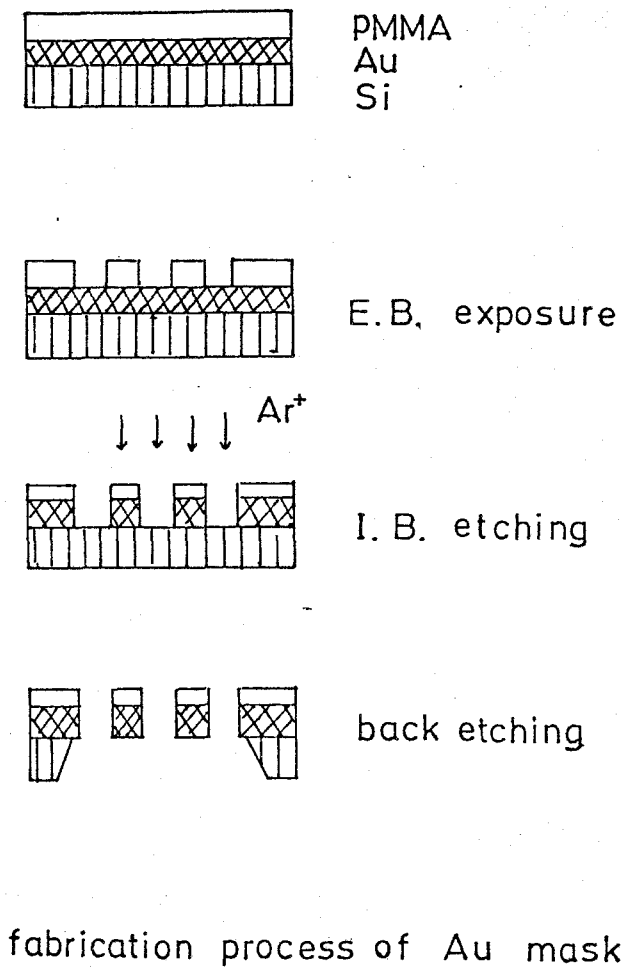

Fig. 2-17. Schematic process fabricating Au free-standing mask for ion beam replication.

Au free-standing-mask of 0.2-0.4 μm thickness was used for the replication of patterns. The Au mask with supporting rim of Si was fabricated by chemical etching of a part of Si substrate under the Au patterns after completing the Au patterns, as shown schematically in Fig. 2-17.

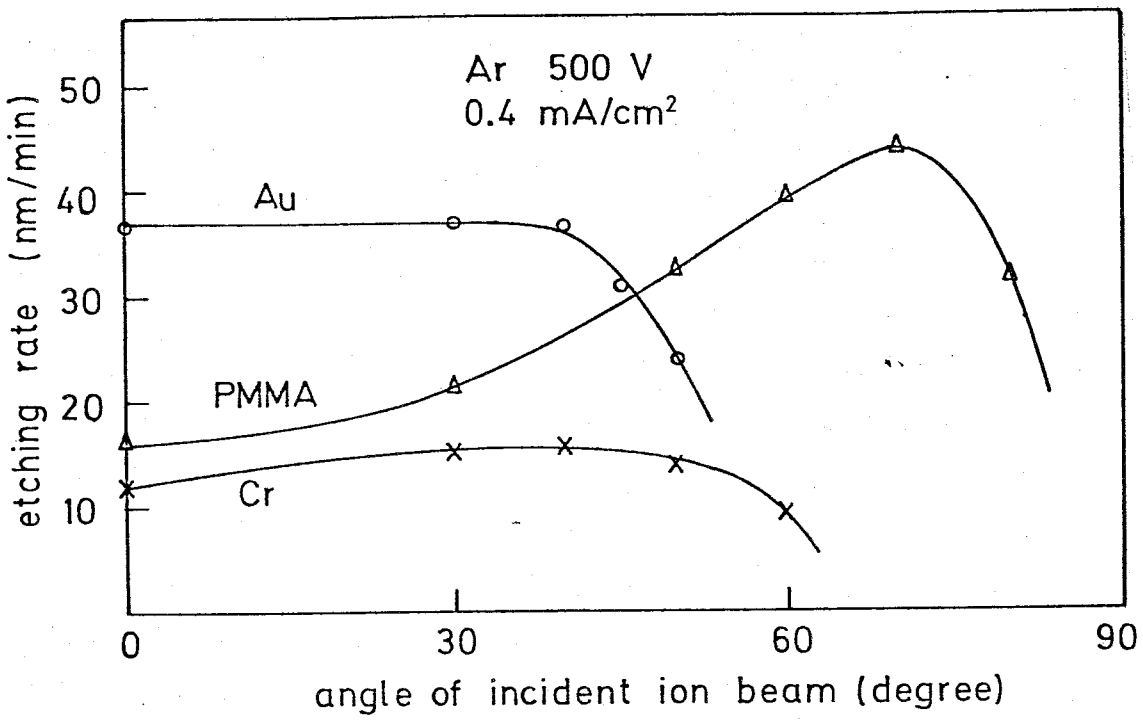

Fif. 2-18. Etching rate of Au, PMMA and Cr for 500 V Ar beam.

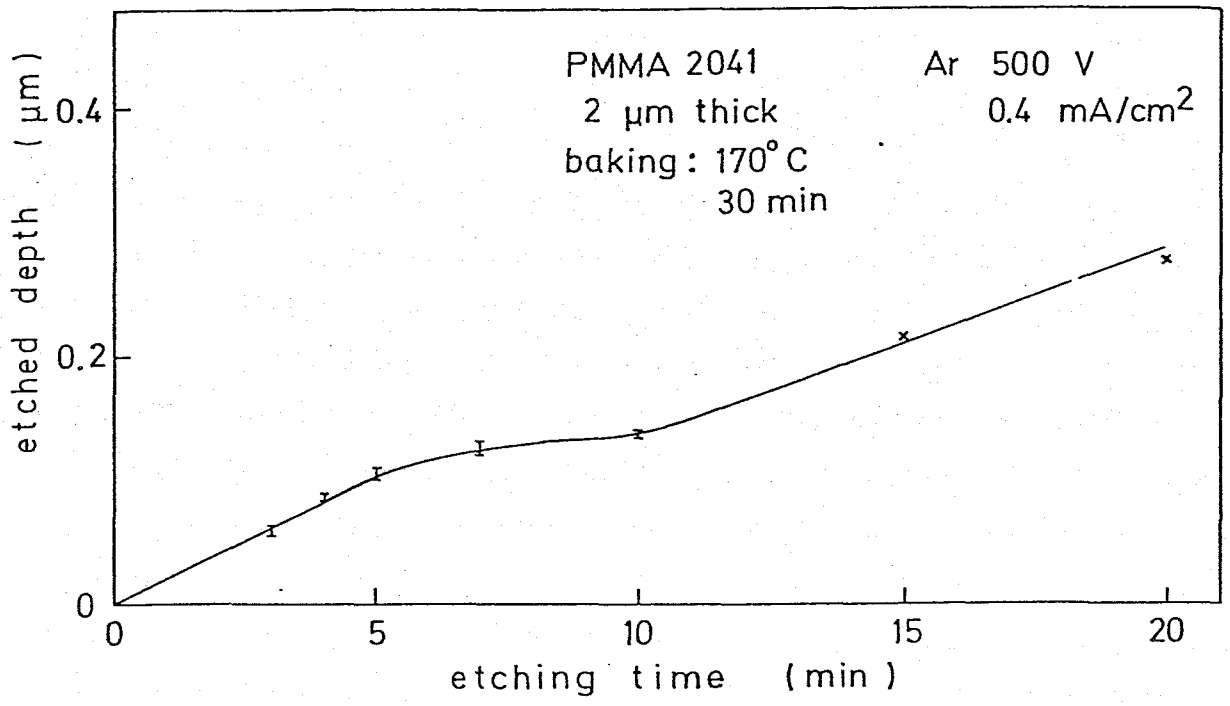

Fig. 2-19. Etched depth of PMMA as a function of etching time.

The Au pattern were fabricated by Ar ion-beam etching or lift off. Figure 2-18 shows etching rate of Au, PMMA and Cr for 500 V Ar ion-beam as a function of the incident beam angle. It is found that etched depth of PMMA increases nonlinearly with etching time after an etching time , as shown in Fig. 2-19. In Fig. 2-19, the etching rate of PMMA is proportionate to etching time until 5 min, but after 5 min the surface of the PMMA resist is found to be deformed like blister due to thermal effect. Therefore, longer etching than 10 min using PMMA mask by the present condition yields very rough edges which is applied to investigate resolution for IBER in the following experiments.

Figure 2-20 are photographs of Au free-standing masks etched by Ar ion beam using PMMA pattern as the etching mask. The PMMA pattern were fabricated by EBL. In Fig. 2-20, the edge of 0.4 μm thick Au pattern is roughened because of longer etching time than 10 min, while 0.14 μm thick Au pattern has smooth edge.

(a)

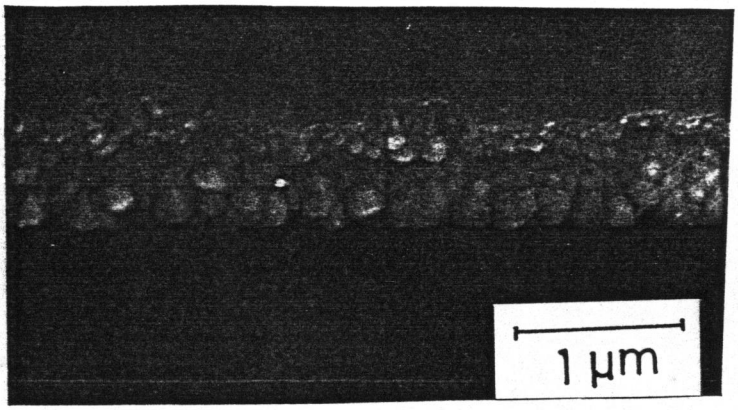

0.4 μm THICK Au

(b)

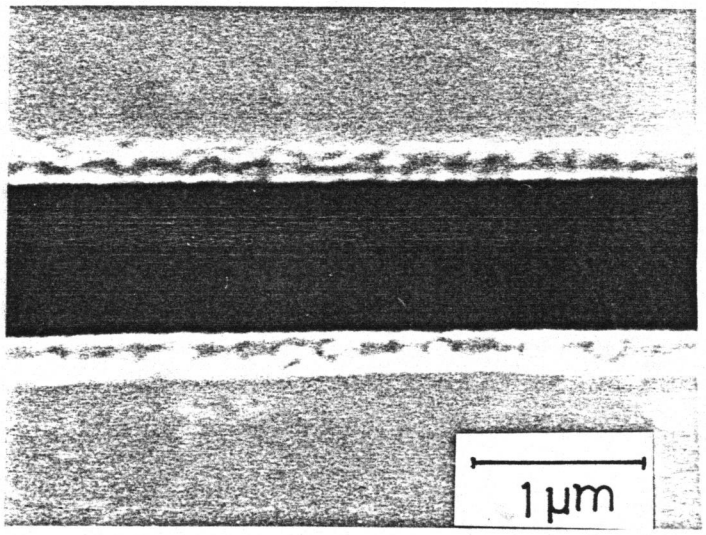

0.14 μm THICK Au

Fig. 2-20. Top view of Au free-standing masks.

2-4-3. Replication of Au Mask-Pattern

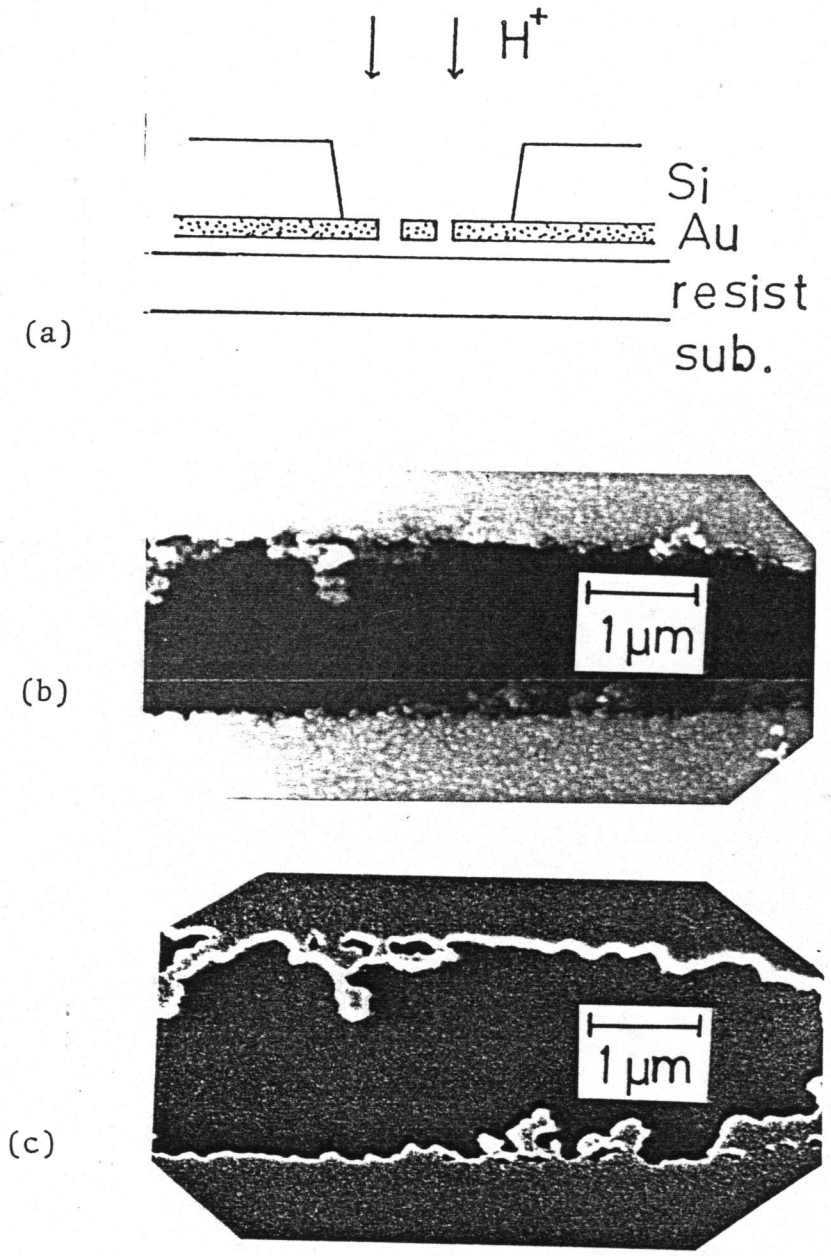

Fig. 2-21. (a) Schematic arrangement of Au mask and wafer and SEM photographs of (b) Au mask (o.4 μm thick) and (c) the replicated PMMA pattern with a dose of $2x10^{-6}$ C/cm^2.

As shown schematically in Fig. 2-21 (a), mask and wafer were in contact with each other during ion irradiation. Figure 2-22 (b) and (c) is SEM photographs of top views of Au mask-pattern and the replicated PMMA pattern, respectively. The thickness of Au pattern is 0.4 μm and is sufficient for the transfer of the pattern with high contrast as is expected from Fig. 2-15. Fine structures of less than 0.1 μm (around 50 nm) at the rough edge of the Au line-pattern was accurately transferred to PMMA and high resolution of this method was confirmed. Figure 2-22 also shows a replicated PMMA pattern which is viewed obliquely to see the side wall of the pattern. The vertical edge of the pattern indicates the scattering of incident ions has small effect on the replicated PMMA pattern.

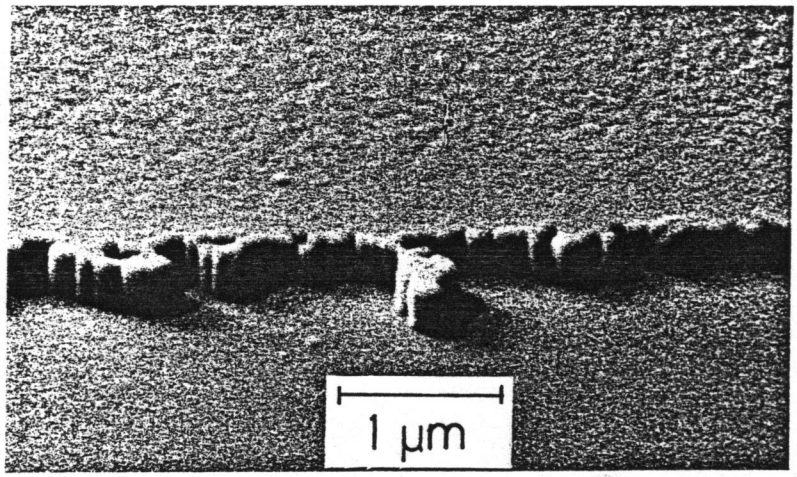

Fig. 2-22. SEM photograph of replicated PMMA pattern using Au mask with rough edge. The sample is tilted to see the side wall. The ion dose was 2×10^{-6} C/cm^2.

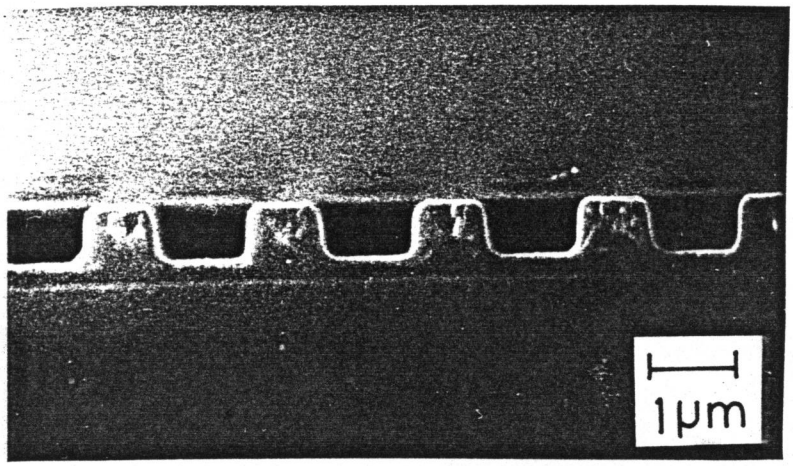

Fig. 2-23. Cross section of the replicated PMMA pattern. The PMMA thickness is thicker than the ion range. The ion dose was 2×10^{-6} C/cm^2.

Figure 2-23 shows a cross section of PMMA pattern which is thick enough to stop all of the incident ions in the resist. Round edges near the groove are seen in the figure, because forward scattering of the ions in the resist cannot be neglected near the end of the ion path. In order to achieve accurate replication, the resist thickness must be taken to be less than about 70 %, judging from Fig. 2-23.

Figure 2-24 compares SEM photographs of the replicated PMMA patterns on Si and Au on Si substrates. The small effect of back scattering of ions in ion beam lithography is clearly seen in the figure. The PMMA line by electron beam lithography is wider on Au on Si than on Si substrates (Fig. 2-24 (a)), while the difference in ion beam lithography is not observed in the photograph (Fig. 2-24 (b)).

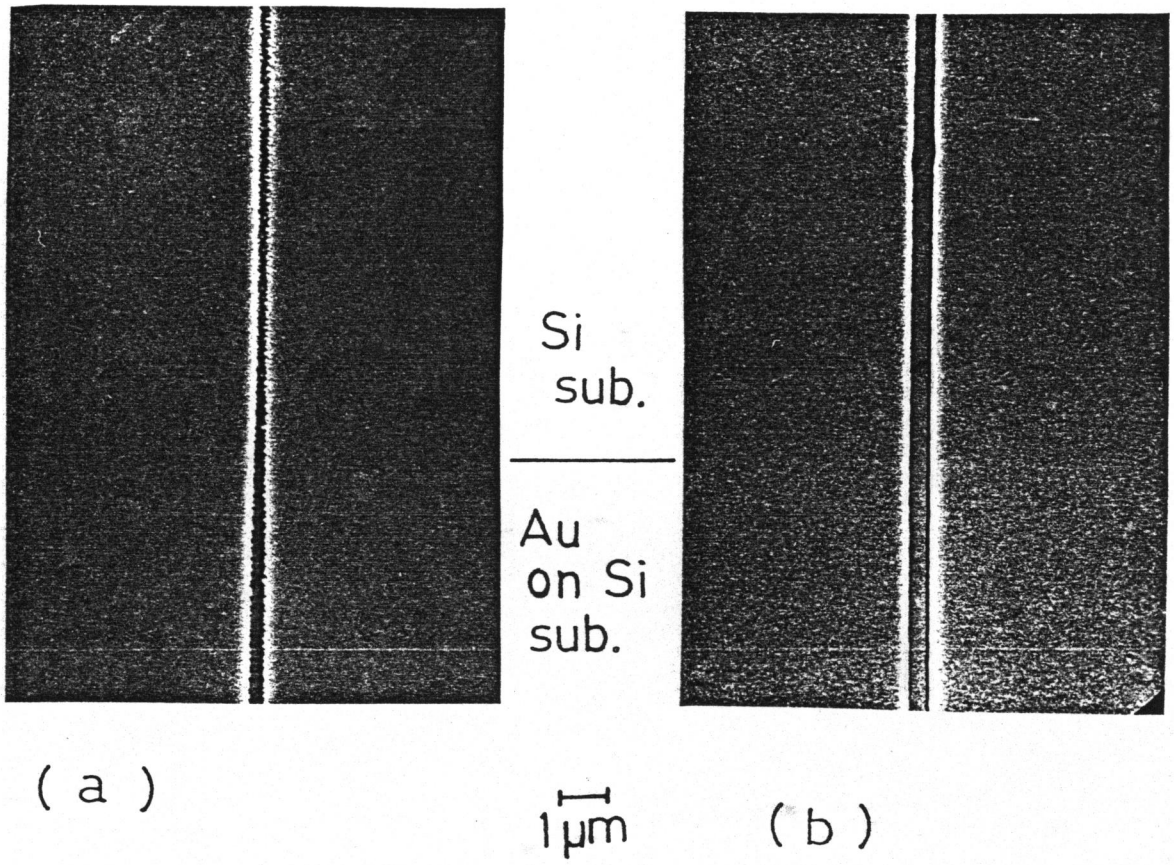

Fig. 2-24. Comparison of PMMA pattern width on Si and Au on Si substrates between (a) electron and (b) ion beam lithography.

2-5. Exposure characteristics of FPM and AZ1350 resists

2-5-1. Introduction

As mentioned in this chapter, IBL is a promising technique to achieve high resolution pattern in resist. On the other hand, very fine patterns in PMMA have been fabricated with a pattern width of 17.5 nm[37] and 16 nm[38] by means of x-ray and electron beam lithography, respectively. These high resolution patterns depend on the excellent property of PMMA which is believed to possess the highest resolution among all resists. Almost all patterns thus far reported having less than 0.1 μm width have been formed in PMMA. By IBL, however, we can expect to fabricate fine lines in a resists other than PMMA with less than 0.1 μm width, utilizing high sensitivity and/or high resistance to dry etching of the resists. This is because the deposited energy spread around the exposed area is little in IBL unlike EBL.

In this section fabrication of fine lines with around or less than 0.1 μm width in FPM (section 2-5-2)[10] and AZ1350 (section 2-5-3)[9] resists is described, as well as the exposure characteristics of the resists such as sensitivity and -value for 50 kev proton beam. The aim of this section is to investigate a possibility to apply various resists other than PMMA to nanometer-lithography by means of IBL.

2-5-2. FPM Resist

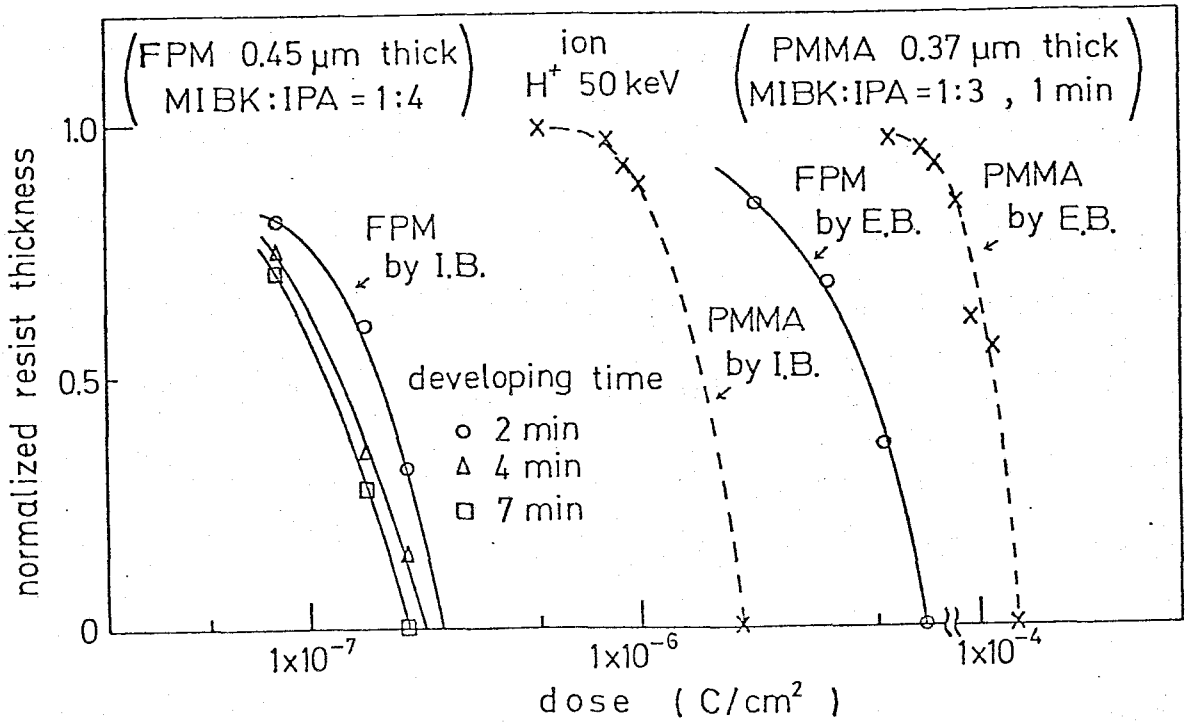

Fig. 2-25. Exposure characteristics of FPM by 50 keV proton beam with a developer of MIBK:IPA = 1:4.

Table 2-2. Sensitivity and γ-value of FPM, PMMA and AZ1350 exposed by 50 keV proton beam.

resist	developer	developing time (min)	sensitivity (C/cm^2)	γ-value
FPM	MIBK:IPA = 1:4	7	2.0×10^{-7}	2.2
	MIBK:IPA = 1:4	4	2.2×10^{-7}	2.2
	MIBK:IPA = 1:4	2	2.6×10^{-7}	2.3
	MIBK:IPA = 1:6	0.5	1.0×10^{-6}	3.3
PMMA	MIBK:IPA = 1:0	2	6.0×10^{-7}	3.0
	MIBK:IPA = 1:1	2	1.5×10^{-6}	3.0
	MIBK:IPA = 1:3	1	2.0×10^{-6}	3.3
AZ1350	AZ devel.	0.5	1.2×10^{-6}	2.2

First, we measured exposure characteristics of FPM by 50 keV proton beam. The results are shown in Fig. 2-25. The sensitivity and the γ-value of FPM are listed in Table 2-2, together with values for PMMA and AZ1350 for comparison. The characteristics of electron-beam exposed FPM were studied at the Ibaraki Electrical Communication Laboratory of NTT. Comparing with the data, the sensitivity of ion beam exposed FPM is 32, 21 and 8.5 times higher than that of electron-beam exposed FPM for developing time of 2, 4 and 7 min, respectively. The γ-value of both electron and ion beam exposed FPM are almost same. The change of the sensitivity of FPM by varying developing time is different between in ion and electron beam exposure. Longer developing time makes the sensitivity increase larger in EBL than in IBER as seen in Table 2-2. This might be due to the larger amount of deposited energy in a resist near the substrate than near the surface because of back scattering effect in EBL.

Another feature evident in Table 2-2 is a slight increase of the γ-value for a weaker developer. This feature is the same as that of PMMA in IBER.[8)]

Though the very high sensitivity of FPM has been demonstrated in Table 2-2, this dose not necessarily lead to achievement of very fine patterns at the dose in Table 2-2. In the case of EBL, sensitivity of a pattern depends on the pattern width due to intraproximity effect. In the present study we attempted to replicate a Au pattern with less than 0.1 μm width in FPM using the process in Fig. 2-26. The Au pattern were formed directly on FPM film using photolithography and oblique

evaporation of Au. The thickness of the obliquely evaporated gold film was 0.15 μm.

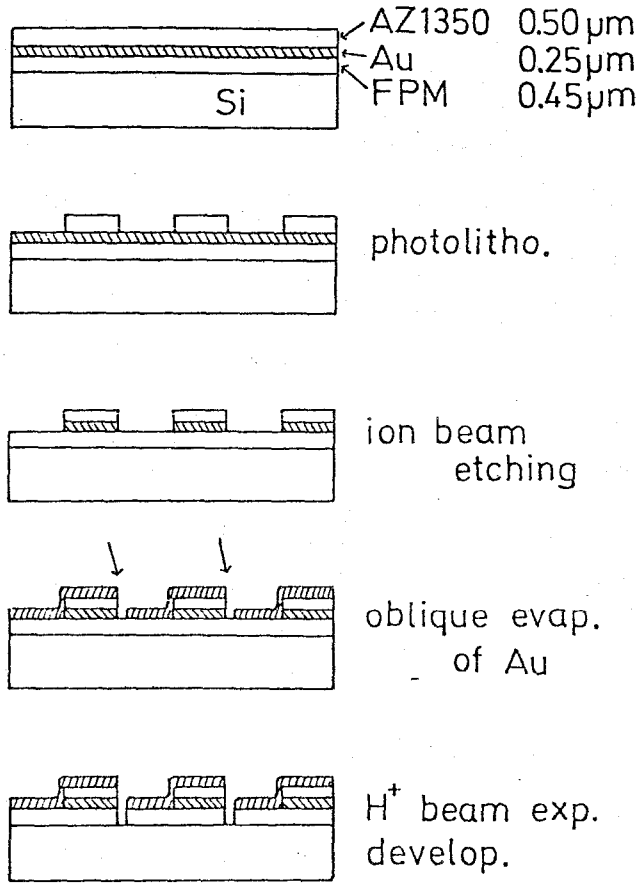

Fig. 2-26. Schematic procerure to fabricate fine lines of FPM by IBER using oblique evaporation technique.

(a)

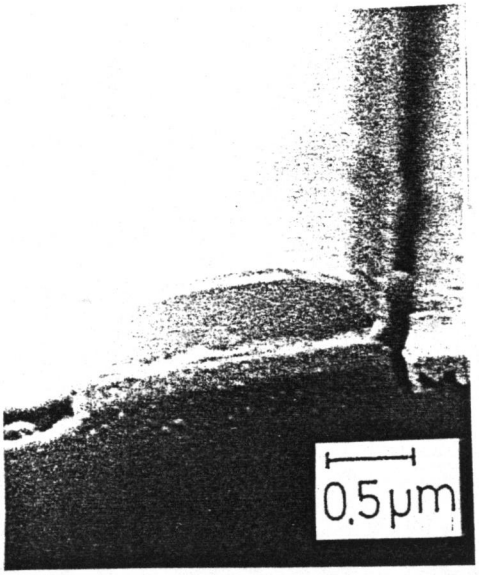

(b)

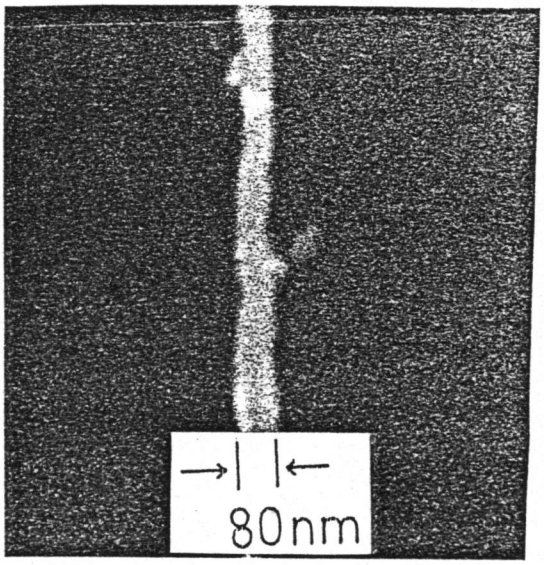

Fig. 2-27. SEM photograph of an FPM pattern with AZ1350 with a dose of 3×10^{-7} C/cm^2, and SEM photograph of Au pattern by lift off using the FPM pattern.

Figure 2-27 (a) is an SEM photograph showing an 80 nm-wide line in FPM with AZ1350 and Au mask after proton beam exposure and development. Figure 2-27 (b) is an SEM photograph of 40 nm-thick Au line after liftoff using the pattern in Fig. 2-27 (a). It is verified that the resolution of 0.2 μm for FPM by conventional EBL is limited by lateral spread of the incident electrons and secondary electrons in the resist, not by the inherent resolution of the resist itself. Because of the small lateral range of the incident ions and secondary electrons in IBER,[5] we have achieved 80 nm-wide lines of FPM resist, though the γ-value is not so high (2.3). Therefore, we can expect to fabricate fine lines with less than 0.1 μm width of various resists other than PMMA to utilize the high sensitivity and/or the high resistance to dry etching of the resists.

Figure 2-28 shows a comparison of dissolution characteristics of FPM between on Si substrate and on Au on Si substrate. No difference has been found between the two substrates in Fig. 2-28. This implies that both back-scattered ions and secondary electrons ejected from the substrate atoms does not affect practically the dissolution characteristics of FPM in IBER. We can expect fine lines like that in Fig. 2-27 on many substrate, because Au has a relatively high level of back scattering ions or secondary electrons among usually adopted substrate materials.

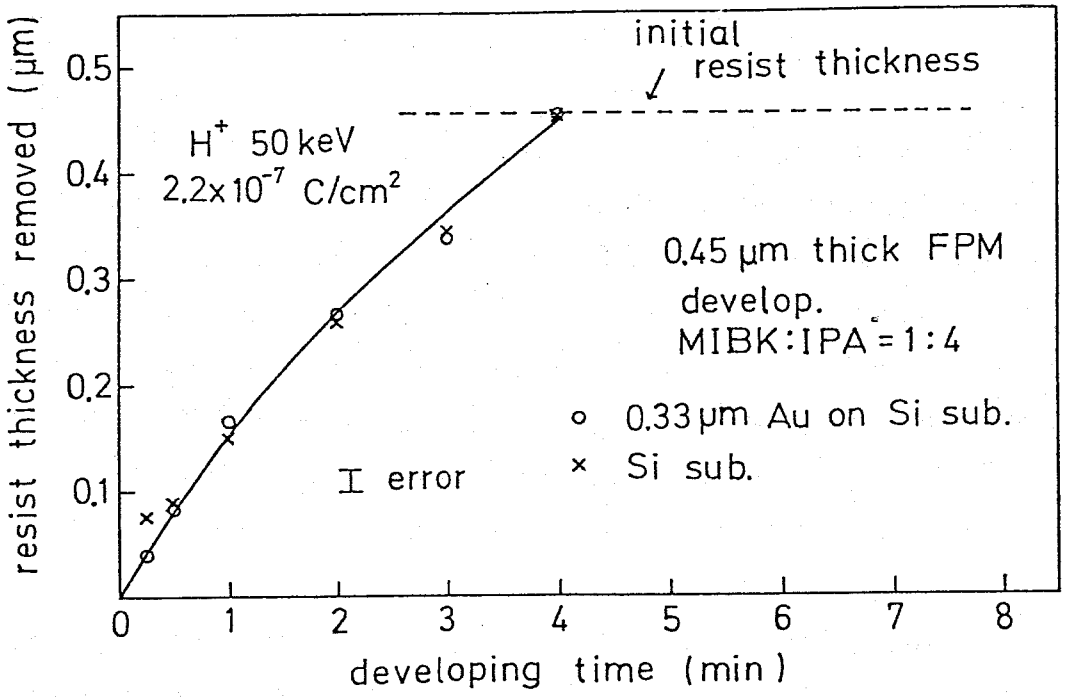

Fig. 2-28. Dissolution characteristics of proton beam exposed FPM on two kinds of substrates.

2-5-3. AZ1350 Resist

Exposure characteristics of AZ1350 resist by 50 keV proton beam are shown in Fig. 2-29. We can see the sensitivity of AZ1350 is almost same as that of PMMA. Dissolution characteristics of AZ1350 shows no difference beween on Au on Si and on Si (in Fig. 2-30), as was seen for FPM in Fig. 2-28. We can also see time lag at the beginning of the development for AZ1350 in Fig. 2-30 unlike FPM or PMMA.

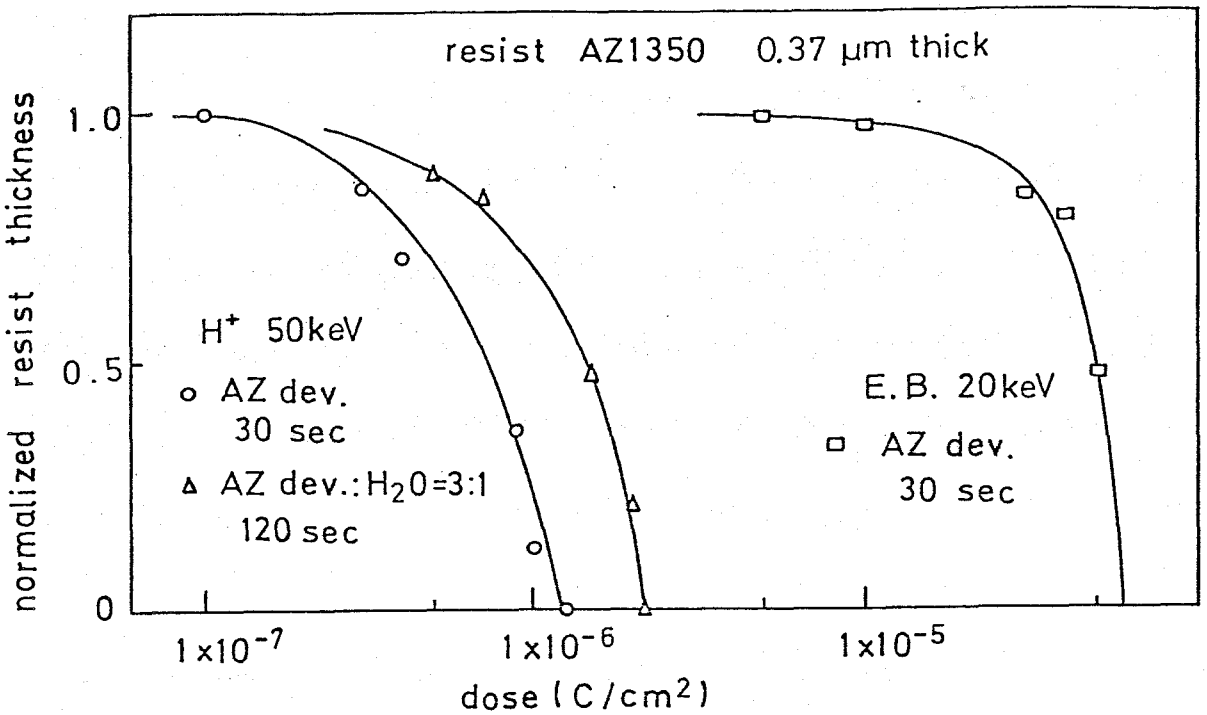

Fig, 2-29. Exposure characteristics of AZ1350 by 50 keV proton beam together with that by 20 keV electron.

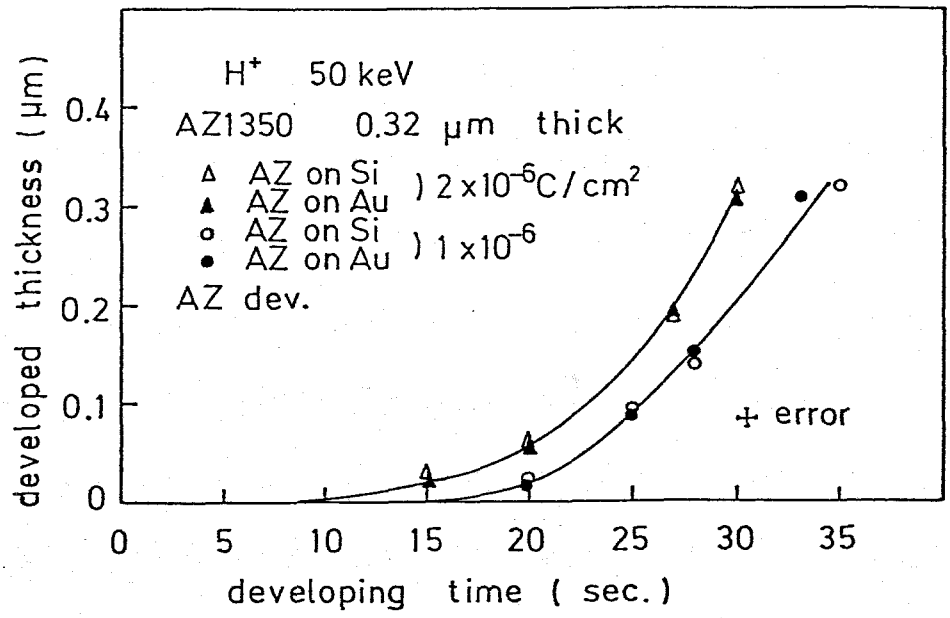

Fig. 2-30. Dissolution characteristics of proton beam exposed AZ1350 on two kinds of substrates.

Figure 2-31 is a schematic procedure used to fabricate AZ1350 pattern by ion beam exposure. Holographic exposure and Ar ion beam etching were adopted to obtain Au grating pattern as a mask on AZ1350 resist. Period of the grating pattern was 0.82 m. Figure 2-32 (a) and 2-32 (b) are SEM photographs of the Au pattern on AZ1350 resist and the replicated AZ1350 pattern without Au mask, made by the process in Fig.2-31. As the samples used in Fig. 2-32 (a) and (b) are not same, the pattern width appeared in the two photographs are not same. We have obtained 0.3-0.4 m wide lines of AZ1350. We can see same magnitude of the edge roughness between the lines in Fig. 2-33 (a) and (b). This imply accurate replication of Au mask pattern to the underlaying resist. We can expect even finer lines of AZ1350. Though we can achieve 0.1 m wide lines of AZ1350 by holographic exposure, cross section of the resist pattern is sinusoidal shape. Therefore, rectangular shape pattern with around 0.1 m width by IBER would be a very useful mask for dry etching of the substrate.

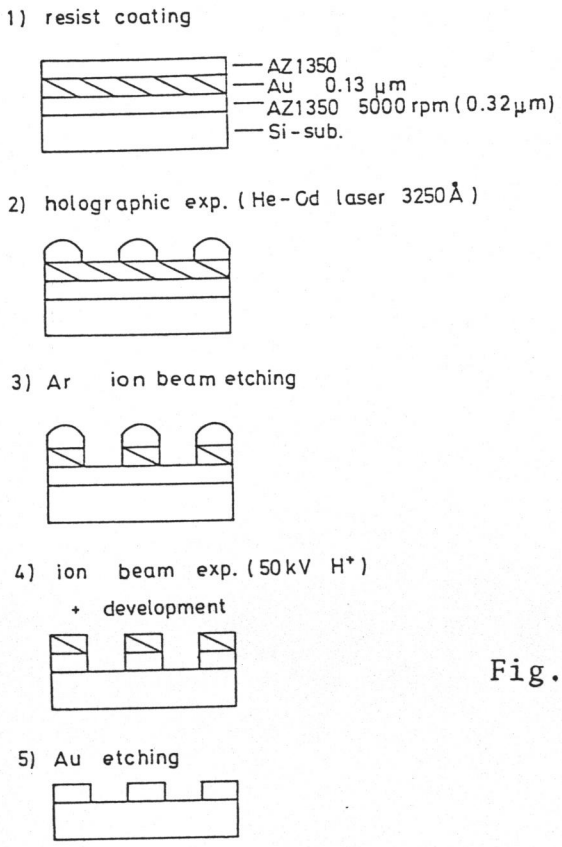

Fig. 2-31. Schematic procedure to fabricate fine AZ1350 pattern.

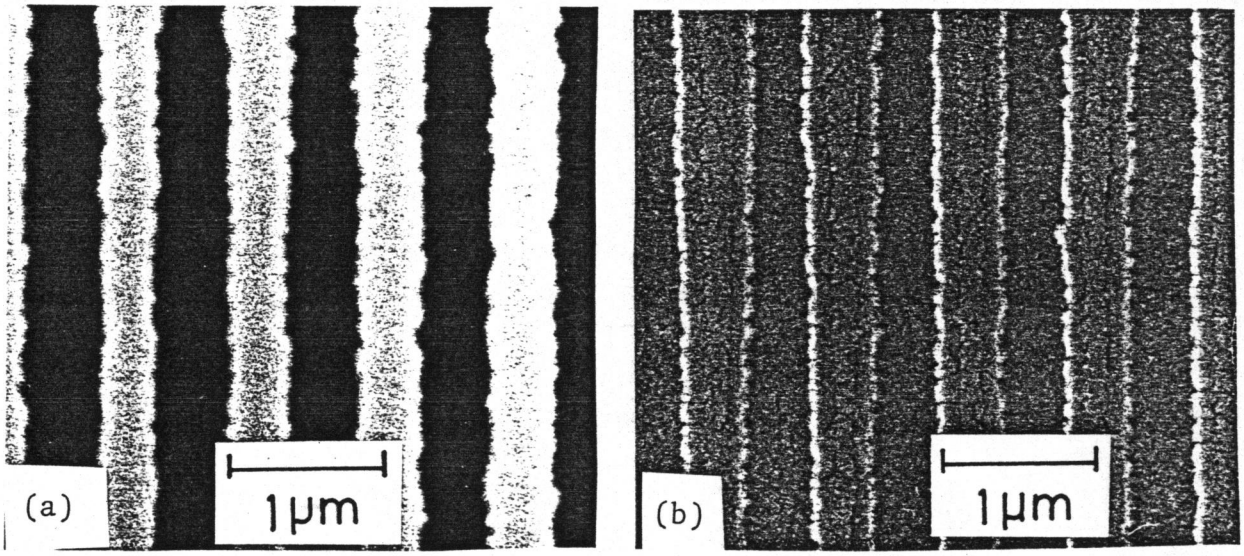

Fig. 2-32. (a) SEM photograph of Au mask on AZ1350 made by holographic exposure. (b) SEM photograph of the replicated AZ1350 pattern.

2-6. Statistical Problems of Impinging ions

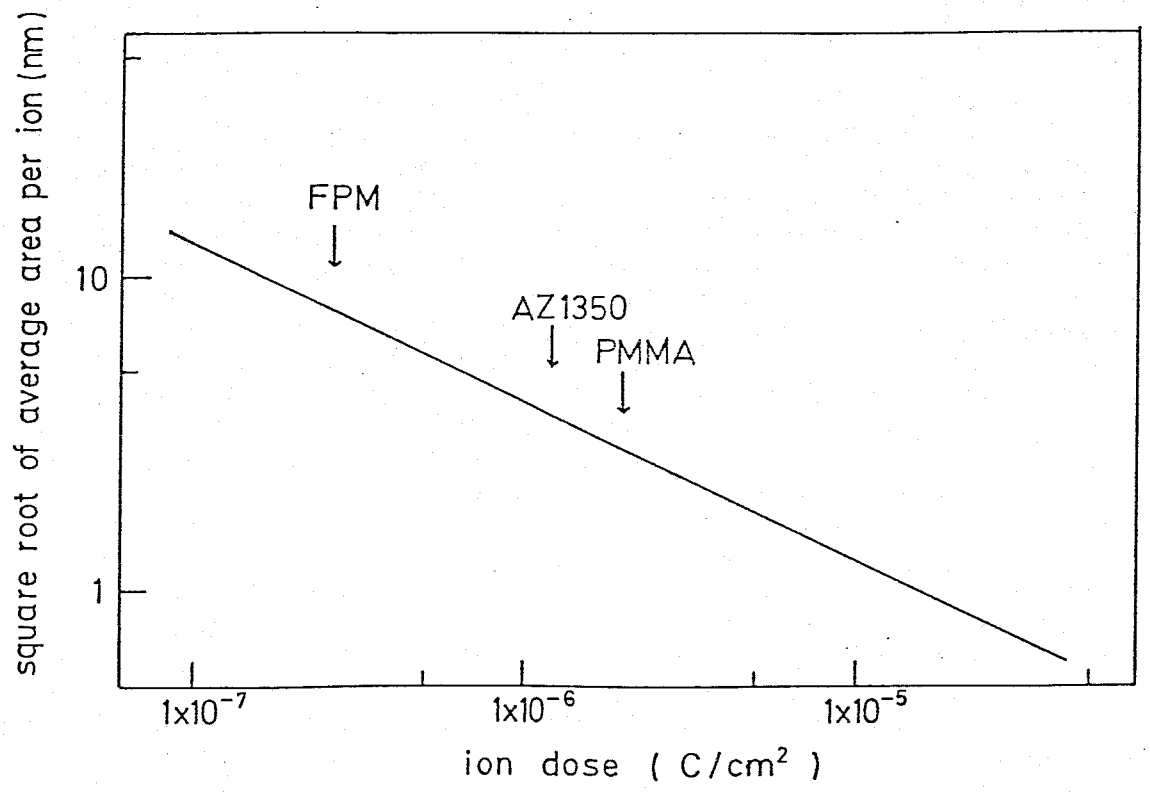

Fig. 2-33. Average area per ion as a function of ion dose. Sensitivity of three resists for 50 keV proton are shown by the arrows.

Figure 2-33 shows a relationship between ion dose and the corresponding average area per ion, together with sensitivities for three resists.

For a resist having both high sensitivity and resolution, we should consider the shot noise effect[5] caused by impinging

ions. The shot noise effect may affect the exposure of FPM resist in a pattern width around 10 nm, because a dose of $3x10^{-7}$ C/cm corresponds to 7.3 nm /proton on average per incident ion.

Figure 2-34 shows estimated probability of underexposure which is defined as less than 60 % of the required dose for the development, as a function of the resolution unit of the resist.

Taking the shot noise effect into consideration, the FPM resist would be appropriate for a pattern size near 0.1 μm using scanning ion-beam lithography in order to make good use of the high sensitivity.

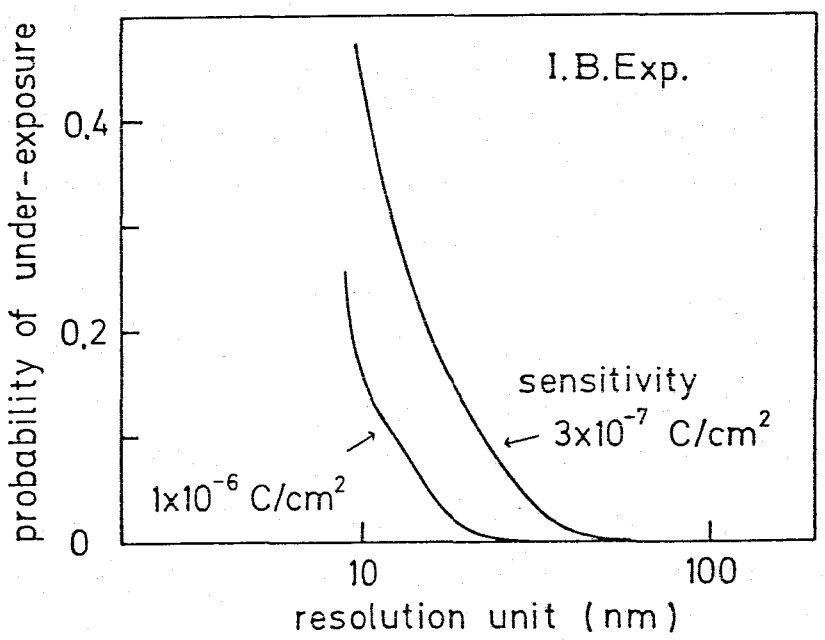

Fig. 2-34. Probability of under-exposure for a resolution unit as a function of the resolution unit. The under exposure is assumed to be 60 % of the sensitivity.

2-7. Conclusions

In this section, results for IBER are summarized.

50 keV proton beam were used to investigate IBER characteristics for PMMA, FPM and AZ1350 resists with an ion implanter.

As for PMMA, the developed depth after proton irradiation was studied in detail. Simple means to calculate the deposited energy profile in the resist was developed using the stopping power and the ion range. Comparing the calculation and experiments, the projected ion range and the standard deviation of the ion range was determined to be 650 nm and 30 nm respectively.

Au free-standing mask was fabricated to demonstrate high resolution of IBER. Fine structures at the edge of the mask pattern was successfully replicated in PMMA accurately with a low dose of $2x10^{-6}C/cm^2$.

IBER for FPM and AZ1350 resists was investigated with regard to its application to nanometrer lithorgaphy. 80 nm wide FPM pattern and 0.3 μm wide AZ1350 pattern were achieved by the replication of Au pattern. The FPM pattern was made with a very low dose of $3x10^{-7}C/cm^2$. FPM would be appropriate to be used in a pattern size near 0.1 μm with scanning ion-beam lithiography, to

make good use of the high sensitivity. AZ1350 would be suitable for a pattern mask to dry etching in a pattern size near 0.1 μm.

In conclusion, excellent features of high sensitivity and high resolution of JBER for fabricating nanometer-structures has been confirmed.

References

1) R.L.Seliger and W.P.Fleming: J. Appl. Phys. 45 (1974) 1416.

2) M.Komuro, N.Atoda and H.Kawakatsu: J. Electrochem. Soc. 126 (1979) 483.

3) L.Karapiperis and C.A.Lee: Appl. Phys. Lett 35 (1979) 395.

4) L.Karapiperis, I.Adesida, C.A.Lee and E.D.Wolf: J. Vac. Sci. Technol. (1981) 1259.

5) D.B.Rensch, R.L.Seliger, G.Csanky, R.D.Olney and H.L.Stover J. Vac. Sci. Technol 16 (1979) 1897.

6) T.M.Hall, A.Wagner and L.F.Thompson: J. Vac. Sci. Technol. 16 (1979) 1889.

7) L.Csepregi, F.Iberl and P.Eichinger: Appl. Phys. Lett. 37 (1980) 630.

8) K.Moriwaki, H.Aritome and S.Namba: Proc. 12th Int. Conf. Solid State Devices, Tokyo 1980, Jpn. J. Appl. Phys. 20 (1981) Suppl. 20-1, 69.

9) K.Moriwaki, H.Aritome and S.Namba: Proc. Microcircuit Engineering 81, Sept. 1981, Lausanne.

10) K.Moriwaki, H.Aritome and S.Nama: Jpn. J. Appl. Phys. 20 (1981) L881.

11) H.Ryssel, K.Haberger and H.Kranz: J. Vac. Sci. Technol. 19 (1981) 1358.

12) N.P.Economou, D.C.Flanders and J.P.Donnelly: J. Vac. Sci. Technol. 19 (1981) 1172.

13) R.L.Seliger, J.W.Ward, V.Wang and R.L.Kubena: Appl. Phys. Lett. 34 (1979) 310.

14) R.L.Seliger, R.L.Kubena, R.D.Olney, J.W.Ward and V.Wang: J. Vac. Sci. Technol. 16 (1979) 1610.

15) G.R.Hanson and B.M.Siegel: J. Vac. Sci. Technol. 16 (1979) 1875.

16) K.Gamo, T.Ukegawa and S.Namba: Jpn. J. Appl. Phys. 19 (1980 L379.

17) H.Kuwano, K.Yoshida and S.Yamazaki: Jpn. J. Appl. Phys. 19 (1980) L615.

18) V.Wang, J.W.Ward and R.L.Seliger: J. Vac. Sci. Technol. 19 (1981) 1158.

19) K.Murase, M.Kakuchi and S.Sugawara: Tech. Paper of Int. Conf. Microlithography, Paris 1977, 261.

20) for example, G.R.Brewer: Electron Beam Lithography in Microelectronic Fabrication (Academic Press, New York, 1980).

21) J.S.Greeneich: J. Appl. Phys. 45 (1974) 5264.

22) J.S.Greeneich: J. Electrochem. Soc. 122 (1975) 970.

23) R.E.Jewett, P.I.Hagouel, A.R.Neureuther and T.Van Duzer: Polymer Eng. Sci. 17 (1977) 381.

24) A.R.Neureuther, D.F.Kyser and C.H.Ting: IEEE Trans. Electron Devices ED-26 (1979) 686.

25) D.F.Kyser and R.Pyle: IBM J. Res. Develop. 24 (1980) 426.

26) R.J.Hawryluk, A.M.Hawryluk and H.I.Smith: J. Appl. Phys. 45 (1974) 2551.

27) D.F.Kyser and K.Murata: IBM J. Res. Develop. 18 (1974) 352.

28) D.F.Kyser and K.Murata: Proc. 6th Int. Cof. Electron and Ion Beam Science and Technology (Electrochemical Society,

New Jersey, 1974) 205.

29) R.Shimizu, T.Ikuta, T.E.Everhart and W.J.Devore: J. Appl. Phys. 46 (1975) 1581.

30) D.F.Kyser and N.S.Viswanathan: J. Vac. Sci. Technol. 12 (1975) 1305.

31) M.Parikh and D.F.Kyser: J. Appl. Phys. 50 (1979) 1104.

32) M.Parikh: J. Appl. Phys. 51 (1980) 705.

33) T.H.P.Chang: J. Vac. Sci. Technol. 12 (1975) 1271.

34) k.Moriwaki, H.Aritome and S.Namba: in preparation for publcation.

35) for example, S.Namba: Ion Implantation Technology (Kogyo Chosakai Publishing Co., Tokyo, 1975) in Japanese.

36) H.H.Andersen and J.F.Ziegler: Hydrogen -Stopping Powers and Ranges in All Elements- (Pergamon Press, New York, 1977) vol 3.

37) D.C.Flanders: Appl. Phys. Lett. 36 (1981) 93.

38) S.P.Beaumont, P.G.Bower, T.Tamamura and C.D.W.Wilkinson: Appl. Phys. Lett. 38 (1981) 436.

39) N.G.Einspruch: VLSI Electronics -Microstructure Science- (Academic Press, New York, 1981).

3. Ion-Bombardment-Enhanced Chemical-Etching (IBECE)

3-1. Introduction

In microfabrication technology various methods have been investigated by which fine patterns with submicrometer dimension can be fabricated. Among them, IBECE is a technique in which an ion-bombarded region on a material is removed by means of enhanced chemical etching as illustrated in Fig. 3-1. After some

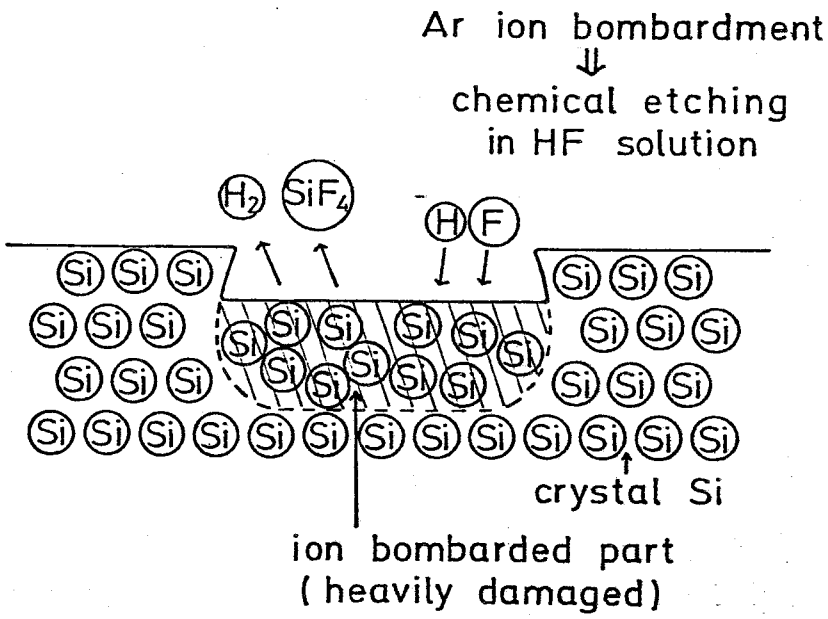

Fig. 3-1. Illustration of IBECE of Si using HF as the etchant.

preliminary experiments,[1,2] Gibbons et al.[3] investigated IBECE in detail and suggested its usefulness as a microfabrication technique. Since then, some fruitful results have been achieved by using this technique which has the advantages of a high level of control for etched depth and is applicable to various kinds of materials.[4-7]

By this technique a high resolution of less than 0.1 μm is expected. In the work so far reported, however, the emphasis has been on the enhanced etching effect rather than on the fine patterning. The pattern width in the previously reported studies was more than a few μm. It is improtant to prove the inherent high resolution of IBECE by fabricating a submicron pattern and investigating the amount of side etching under the mask.

Moreover, direct engraving of submicron patterns using IBECE without mask is an attractive process which would be realized with focused type IBL system.

In this chapter basic characteristics of IBECE for Si[9,10] (in the section 3-3) and SiO_2[10] (in the section 3-5) using HF solution as the chemical etchant have been studied to demonstrate the above-mentioned advantages of IBECE as a means for nanometer lithography. Particularly for Si, The etched profile under a mask is investigated in detail with 10 nm accuracy[11] in the section 3-4. The resolution of IBECE is also dicussed in the section 3-4.

3-2. Experimental Procedure

Table 3-1, IBECE condition for Si.

ION	Ar^+
ACC. VOL.	60 kV
DOSE	3.2×10^{-5} - 8.0×10^{-4} C/cm^2
DOSE RATE	0.3 - 1.0 $\mu A/cm^2$
SUBSTRATE	n-type (100)face Si
ETCHANT	diluted HF 4.7 %, R.T.
ETCHING TIME	3 - 5 h

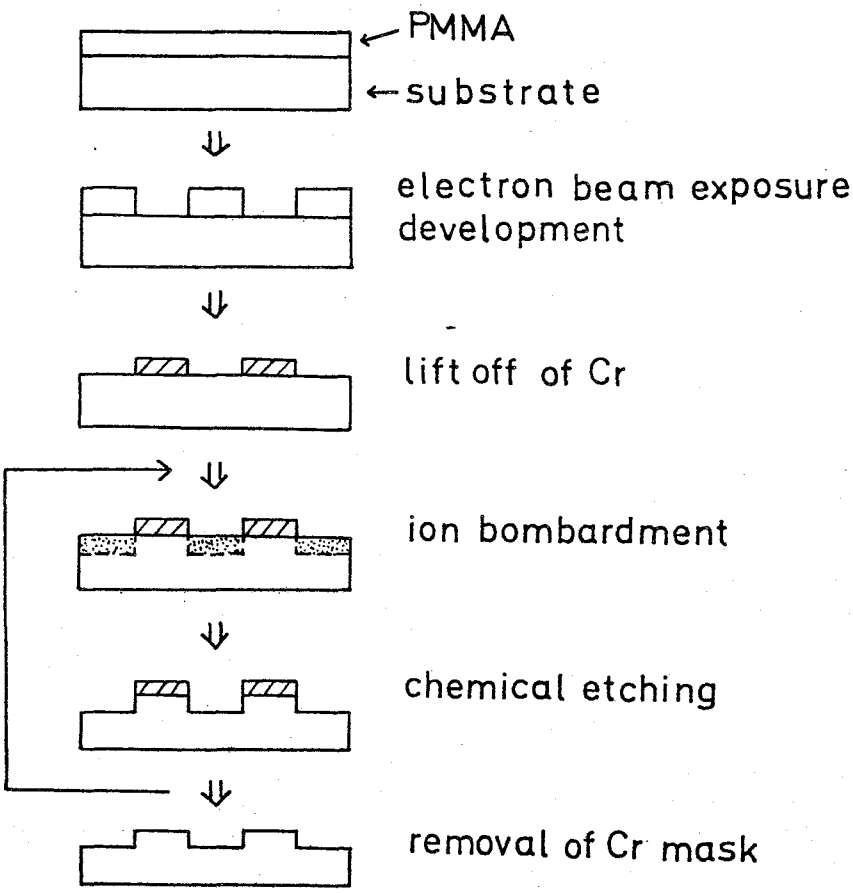

Fig. 3-2. Schematic process for fabricating patterns by IBECE.

Si and SiO_2 were etched by IBECE using 60 keV Ar ion as the bombarding ion with an ion implanter (in Fig. 2-3) and using HF solution as the etchant.

Table 3-1 summarizes the etching condition for Si. For SiO_2, the same conditions were employed except 0.47 % HF as the etchant and less than 30 min for the etching time.

Figure 3-2 shows the schematic procedure used in this experiment for the fabrication of fine patterns in n-type Si wafers of (100) face and in fused quartz. PMMA patterns (0.37 μm thick) were prepared by electron beam lithography (in Fig. 2-4) and were transferred to 0.12 - 0.17 μm thick Cr film by the lift-off technique. In the case of SiO_2, 20 nm thick Au were coated on the surface of PMMA to avoid charging during the electron beam irradiation, and were etched before the development. Samples were bombarded by 60 keV Ar ions and were tilted 5-10° from the direction of the incidnet Ar beam in order to avoid the channeling effect, and were partially covered for measurements of the etched depth. Ion-bombarded Si and SiO_2 was etched by a diluted HF solution. An interference microscope and a scanning electron microscope (SEM) were used to measure the etched depth and the etched pattern, respectively.

3-3. IBECE characteristics of Si

The etched depth is shown in Fig. 3-3 as a function of HF concentration. The etched depth shows the maximum by using 4.7 % HF solution which was used hereby throughout the present

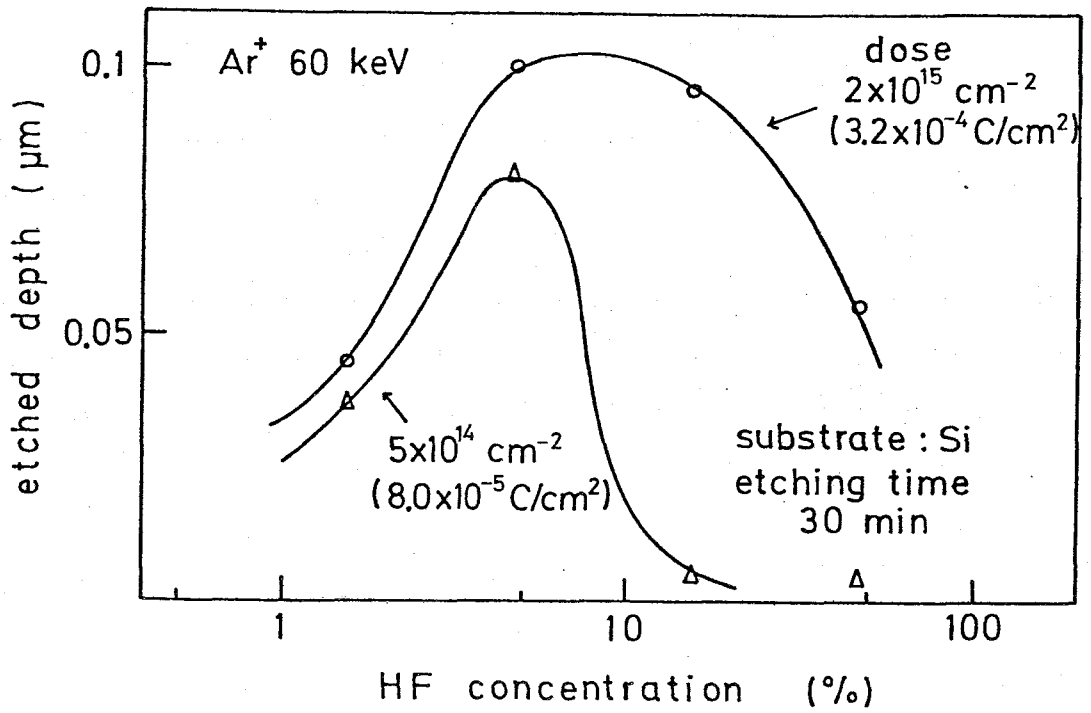

Fig. 3-3. Etched depth of Si by IBECE as a function of HF concentration.

experiments.

The etched depth is shown in Fig. 3-3 as a function of the etching time. It is very improtant that the eched depth saturates after a sufficiently long etching time in IBECE. The saturated etched depth is mainly determined by the damaged thickness in the substrate and is hardly affected by the chemical etching condition in contrast with the usual chemical etching technique. However, the temperature of the etchant in IBECE alters the etching time for saturation and also slightly changes the saturated etched depth.[5,6] By using a proper etchant which

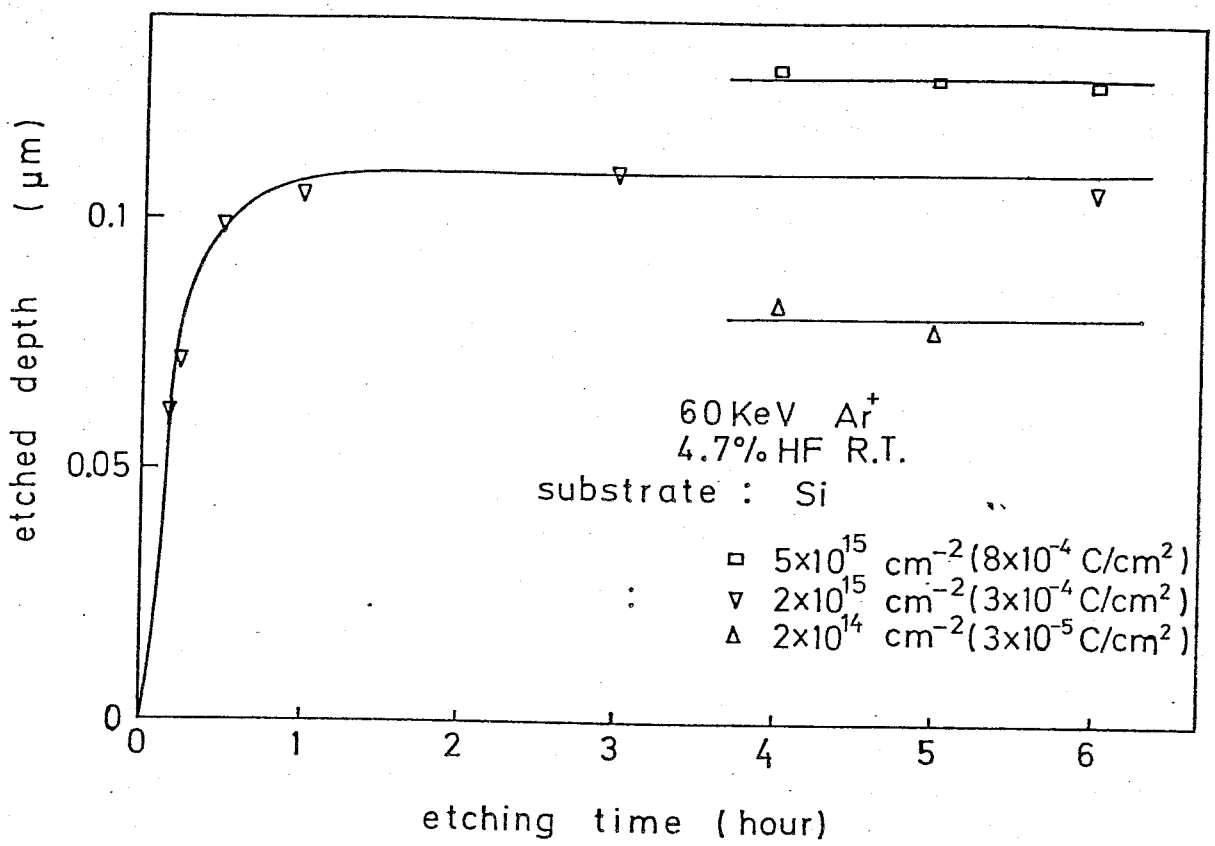

Fig. 3-4. Etched depth of Si as a function of etching time.

hardly etches the unbomabrded region, the ratio of etching rates between the bombarded and unbombarded regions in Si can be several hundred. Diluted HF was found to be a suitable etchant of Si for the lithographic use of IBECE, in which the etching rate of unbombarded Si was 0.2 - 0.5 nm/h and that of ion-bombarded Si was 0.1 μm/h (in Fig. 3-4).

The saturation phenomenon of the etched depth in Fig. 3-4 indicates the existence of a threshold corresponding to the transition from crystal to amorphous or heavily damaged state due to ion bombardment. Existence of the threshold is of great importance because the threshold value defines the etched surface profile. The damaged layer thickness in an ion-bombarded Si substrate can be evaluated as an energy density deposited in the Si substrate by means of nuclear collision between bombarding ions and substrate atoms.

Figure 3-5 shows depth profiles of deposited energy in Si with some doses of 60 keV Ar calculated by LSS theory.[12] It is assumed that the enhanced etching occurs above a certain threshold energy.[6] By taking a value of 4×10^{23} eV/cm^3 as the threshold, the etched depth is calculated to be 95 nm at a dose of 5×10^{14}Ar/cm^2, 104 nm at a dose of 1×10^{15} Ar /cm^2 and 110 nm at a dose of 2×10^{15} Ar /cm^2 , and these are compared with the experimental results as shown in Fig. 3-6. The result verifies the existence of the threshold and the high level of control of etched depth by varying the ion dose with an experimental error of 10 nm in the dose range of 2×10^{14} 5×10^{15}Ar /cm^2.

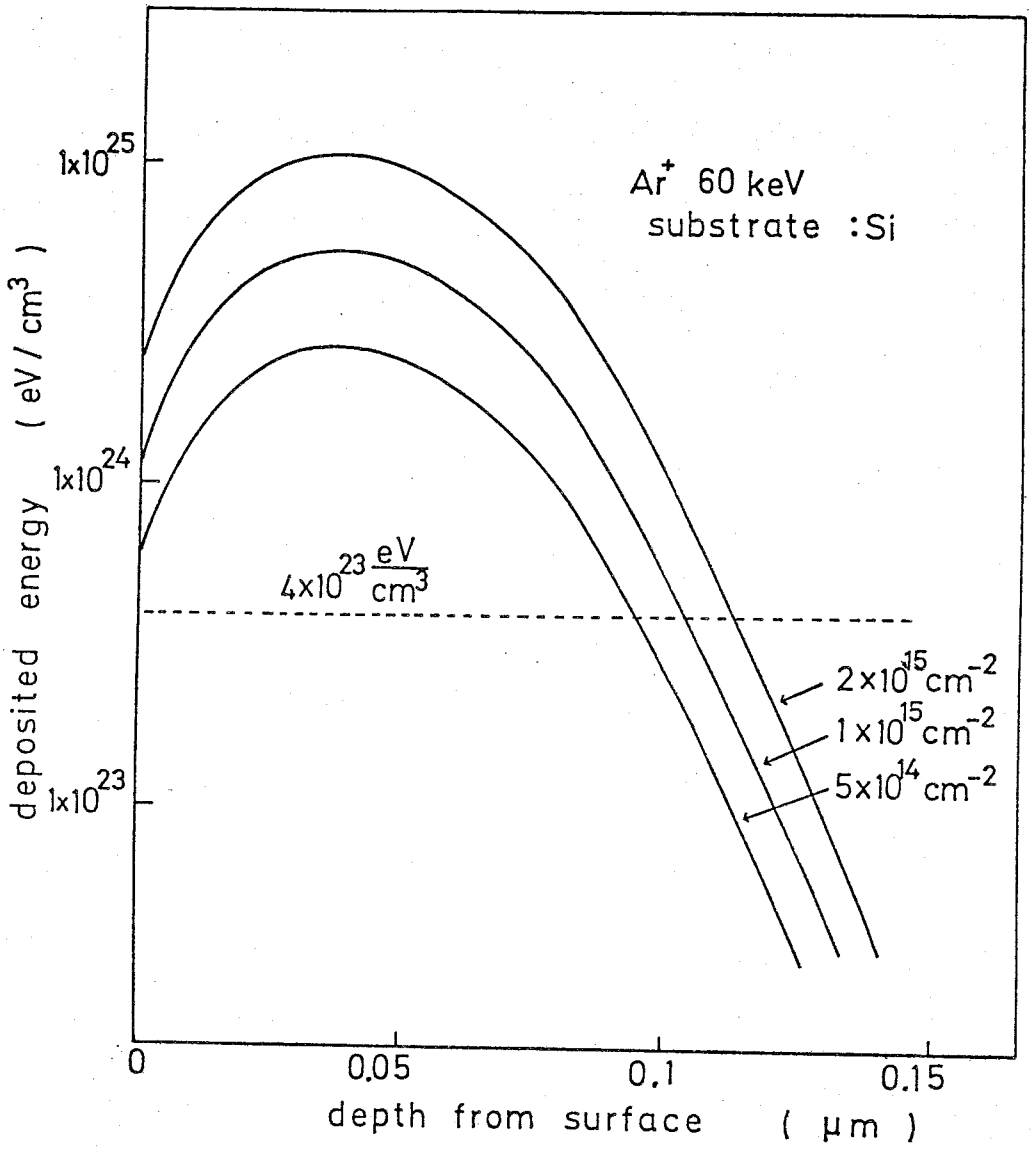

Fig. 3-5. Calculated depth profile of deposited energy in Si bombarded by 60 keV Ar.

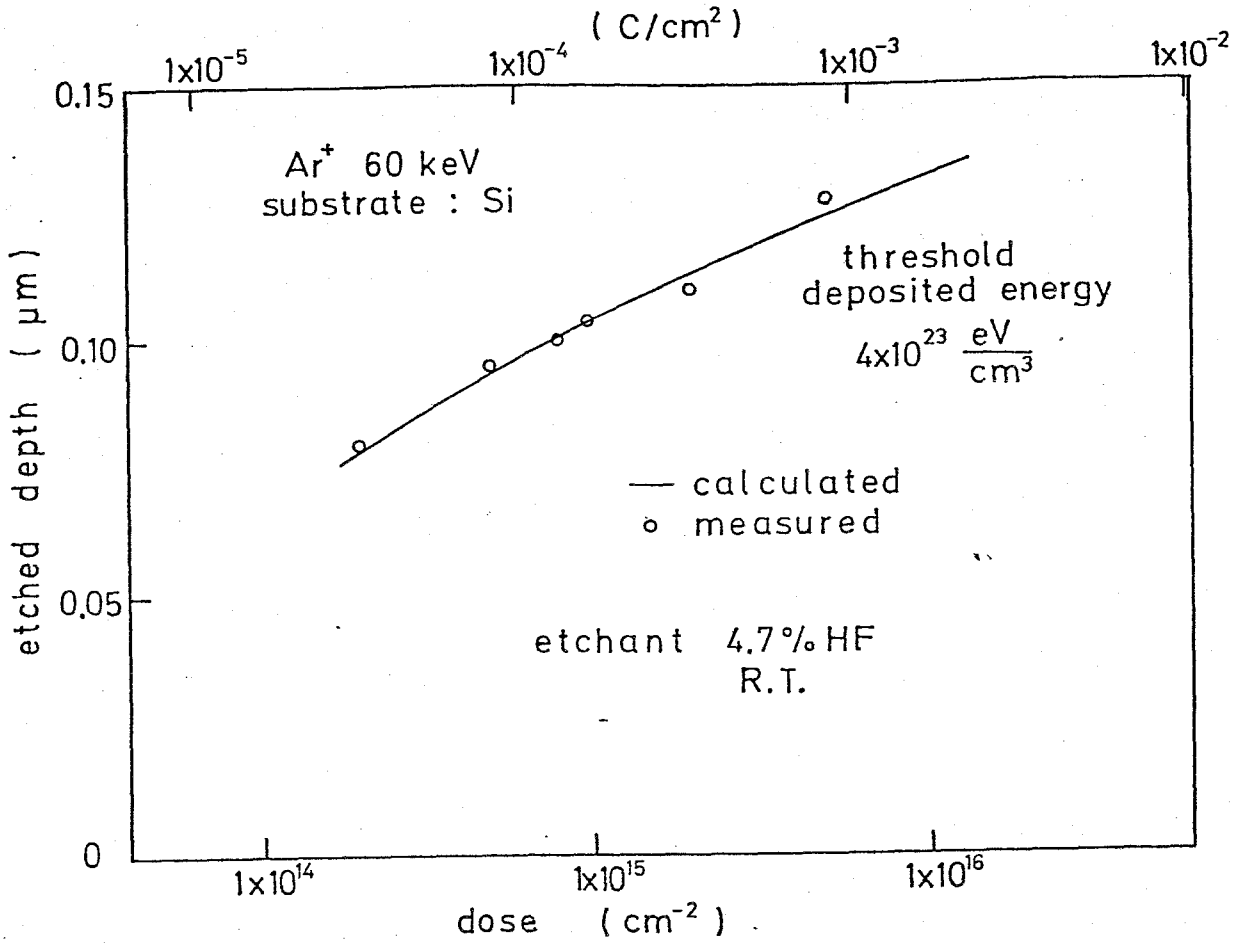

Fig. 3-6. Etched depth of Si as a function of ion dose.

The threshold energy density of the transition from crystalline to amorphous layer in Si is 5×10^{23} eV/cm^3 [13] which closely corresponds to the assumed threshold value in Fig. 3-5. The threshold deposited energy is influenced by several experimental factors. For example, temperature rise of Si substrate at a high dose rate during ion bomabrdment might increase the threshold value.[14] This, however, occurs only at very high dose rates, and at a dose rate of less than 1×10^{13}/cm^2 s which was used in these experiments, the etched depth was independent of dose rate. The obtained value of the threshold energy density in this experiment enable calculation of the etched surface profile of Si which is very important for device application and for estimating the side etching.

3-4. Pattern Profile of Si

3-4-1. Introduction

As mentioned in the previous section, by taking a value of 4×10^{23} eV/cm^3 as the threshould, the change in etched depth as a function of the ion dose was estimated from a calculation of the depth profile of the deposited energy density in Si to an accuracy of 10 nm.

It is very important to investigate the resolution of IBECE and the etched profile under a mask pattern for the application of IBECE to nanometer lithography.

In the present section, the lateral spread of damage induced by bombarding ions is calculated (in the section 3-4-2) as well as the depth profile.[11] The calculated profile is compared with oberved one in the section 3-4-3. And the sections 3-4-4 and 3-4-5 describe the optimum condition and resolution for IBECE.

3-4-2. Calculation of Etched Profile

As mentioned in the previous section, by taking a value of 4×10^{23} eV/cm^3 as the threshould, the change in etched depth as a function of the ion dose was estimated from a calculation of the depth profile of the deposited energy density in Si to an accuracy of 10 nm.

In this section, the etched profile was calculated assuming that the mask has a vertical edge and sufficient thickness to stop the insident ions using a coordinate illustrated in Fig. 3-7.

Though the standard deviation of lateral damage-spread changes with depth from the surface in a rigorous treatment,[15] a constant value of 27.0 nm was used in the calculation.

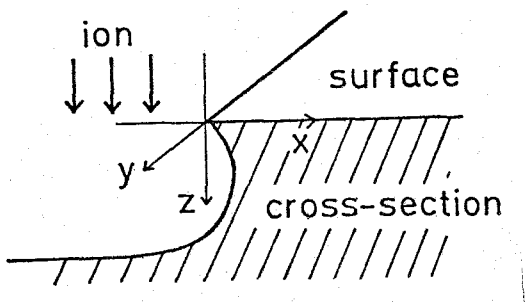

Fig. 3-7. Coordinate for Calculating deposited energy distribution under a mask.

At a point (x,y,z) in the Si substrate, the deposited energy density is represented by[15)]

$$N_d(x,y,z) = \iint_{\infty}^{\infty} D(u,v)\cdot A(z)\cdot \exp\left(-\frac{u^2+v^2}{2\ L_d^2} \right) du\ dv, \quad (3\text{-}1)$$

$N_d(x,y,z)$: deposited energy density by nuclear collision (eV/cm^3)

$A(z)$: depth profile of deposited energy density per electron (eV/cm^3)

L_d: standard deviation of lateral spread of deposited energy density (cm)

$D(x,y)$: surface distribution of incident ion-dose (cm^{-2}).

In the following part of this section, N_d (x,y,z) is calculated using three kinds of D(x,y).

a) uniform dose:

If the dose distribution is uniform,

$$D(x,y) = D_0 \ : \text{constant}, \quad (3\text{-}2)$$

and $N_d(x,y,z)$ is simply given by

$$N_d(x,y,z) = 2\cdot L_d^2\cdot D_0\cdot A(z) \equiv P(z), \quad (3\text{-}3)$$

where P(z) is calculated from LSS theory by using a modified Gaussian function.[12)]

b) under a thick mask with a vertical edge:

If

$$D(x,y) = D_0, \quad x \leqq 0$$
$$= 0, \quad x>0 \tag{3-4}$$

then N_d is calculated to be[15)]

$$N_d(x,y,z) = P(z)\cdot \mathrm{erfc}(\frac{x}{L_d}), \tag{3-5}$$

where

$$\mathrm{erfc}(t) \equiv \frac{1}{\sqrt{2\pi}} \int_t^{\infty} \exp(-\frac{w^2}{2})\, dw. \tag{3-6}$$

c) focused ion-beam with Gaussian edge-profile

If

$$D(x,y) = D_0, \quad x \leqq 0$$
$$= D_0 \exp(-\frac{x^2}{2\sigma^2}), \quad x \geqq 0 \tag{3-7}$$

then

$$N_d(x,y,z) = P(z)\cdot \mathrm{erf}(\frac{x}{L_d}) + \frac{P(z)}{\sqrt{1+\kappa^2}}$$
$$x \exp(-\frac{x^2}{2\ {}^2(1+\kappa^2)})\cdot \mathrm{erfc}(-\frac{x}{L_d\sqrt{1+\kappa^2}}), \tag{3-8}$$

where

$$\kappa \equiv \frac{L_d}{\sigma}.$$

3-4-3. Observed Etched Profile

Figure 3-8 shows calculated profiles of Si by IBECE at a pattern edge using eq. (3-5). The etched profile has a unique feature, i.e. a bending profile at the surface is presented corresponding to the fact that the lateral spread of damage by incident ions is a maximum at a certain depth from the surface. The bending profile is unique, and is unlike that in other etching techniques such as ion beam etching and chemical etching.

The actual etched pattern of Si was influenced by ions through the inclined wall of the mask edge (a typical tilt-angle of Cr mask edge was 70-80°). It was found that the effect is only to change the Si profile a little at the surface. At doses of more than $5x10^{15}$ Ar/cm^2, the influence of ions through the mask was not observed because the amount of lateral damage-spread was sufficiently large in comparison with the ion range through the mask. Figure 3-9 shows an SEM photograph of the etched Si and the calculated profile at a dose of $5x10^{15}$ Ar/cm^2 . The calculated profile is in good agreement with the observed one. The profiles at low doses can be seen in Fig. 3-10 in which the surface bending profile like in Fig. 3-8 is hardly found.

IBECE is expected to become a useful technique for direct etching of substrates without mask by using such an ion beam system. By assuming a Gaussian distribution of the incident ion beam, the etched profile of Si are calculated using eq. (3-8) in Fig. 3-11 and Fig. 3-12 for maskless etching. The ion dose is varied in Fig. 3-11 and the dose distribution is varied in

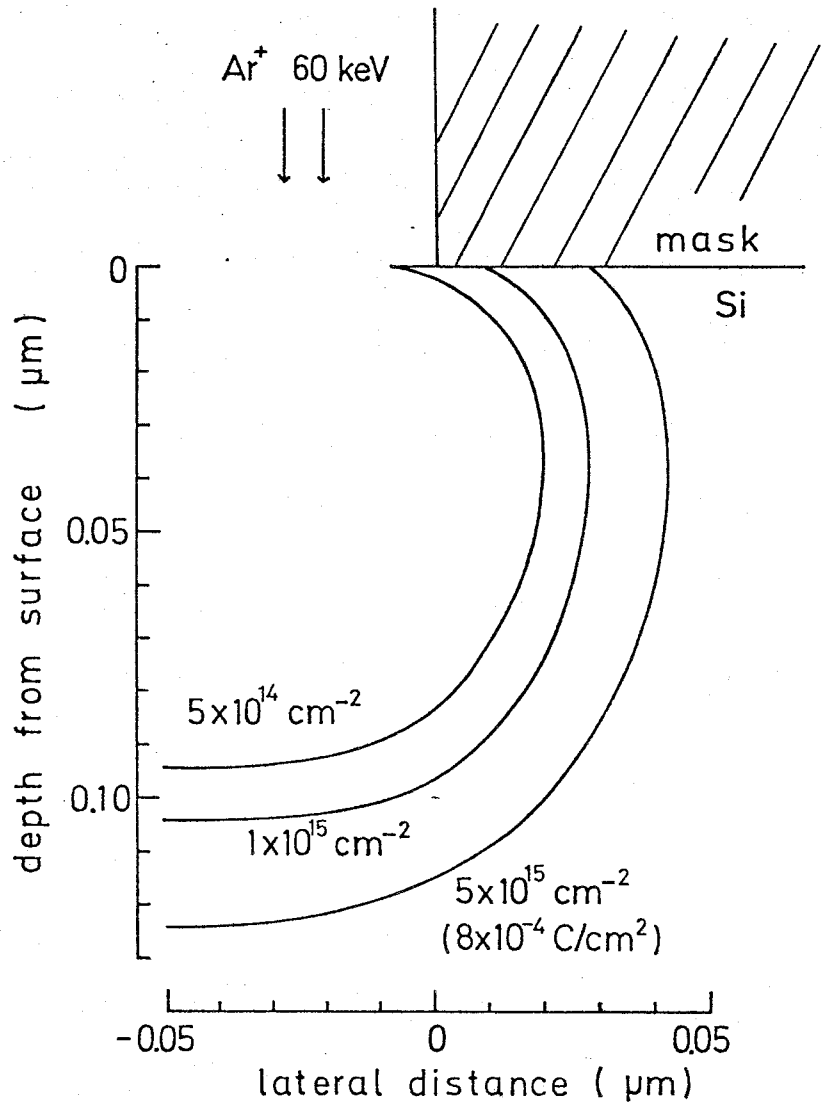

Fig. 3-8. Calculated etched profile of Si at the pattern edge. The etched profile is obtained by calculating the deposited energy density in Si using the threshold energy density.

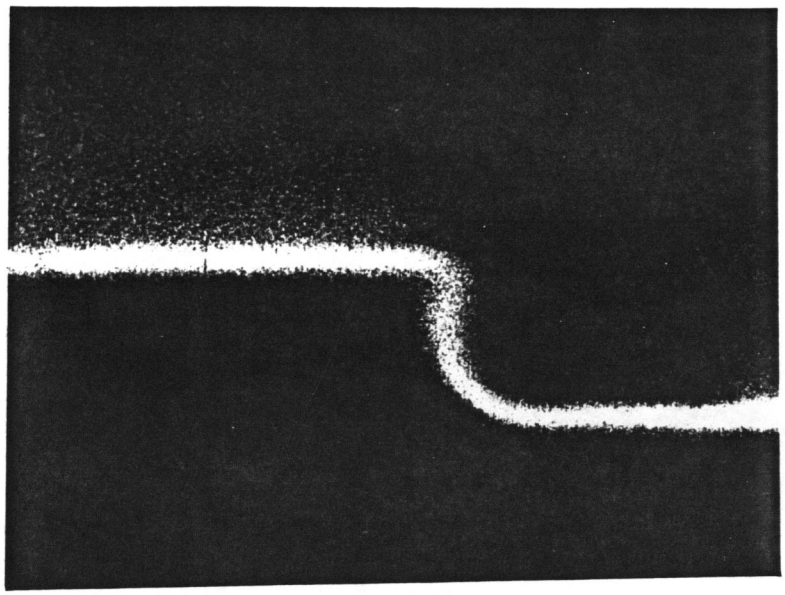

SEM photo.

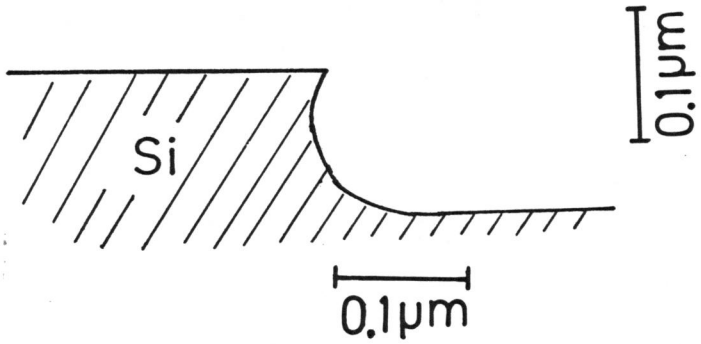

calculated profile

Ar^+ 60 keV , 5×10^{15} cm^{-2}
(8×10^{-4} C/cm^2)

Fig. 3-9. Comparison of observed and calculated profiles of etched Si at a pattern edge. The Cr mask has been etched away.

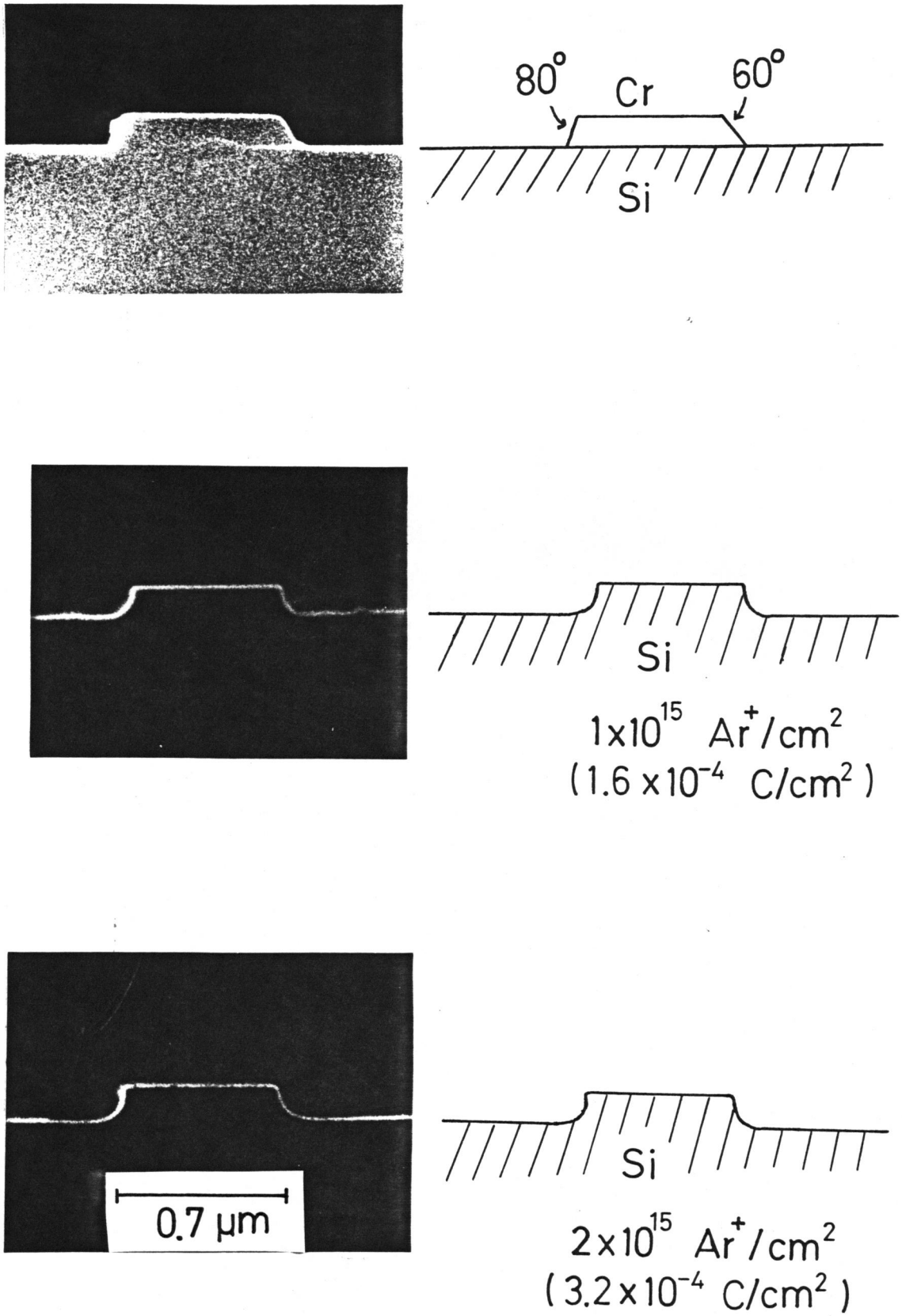

Fig. 3-10. Cr mask and the replicated Si patterns by IBECE. Dependence of Si profile on the Cr mask wall-angle can be seen.

Fig. 3-12. It can be seen that the defocusing effect of the incident ion beam causes an increase in the curvature of the etched Si profile in Fig. 3-11, while an increase of the dose hardly change the Si profile but shifts it toward the interior of the substrate in Fig. 3-12. The etched profile is very easily predicted in IBECE.

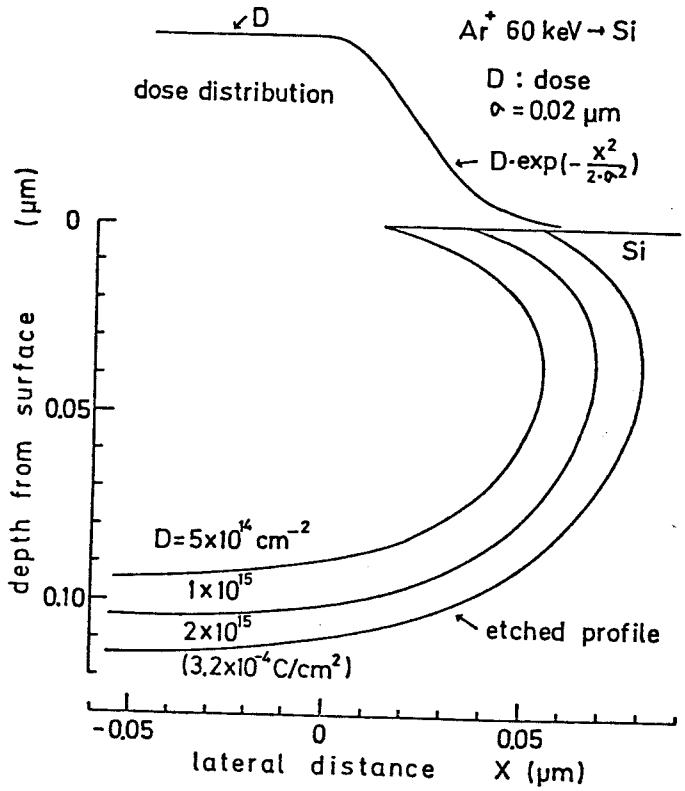

Fig. 3-11. Calculated etched profile of Si by IBECE using incident ion-beam of Gaussian distribution. Ion dose is varied.

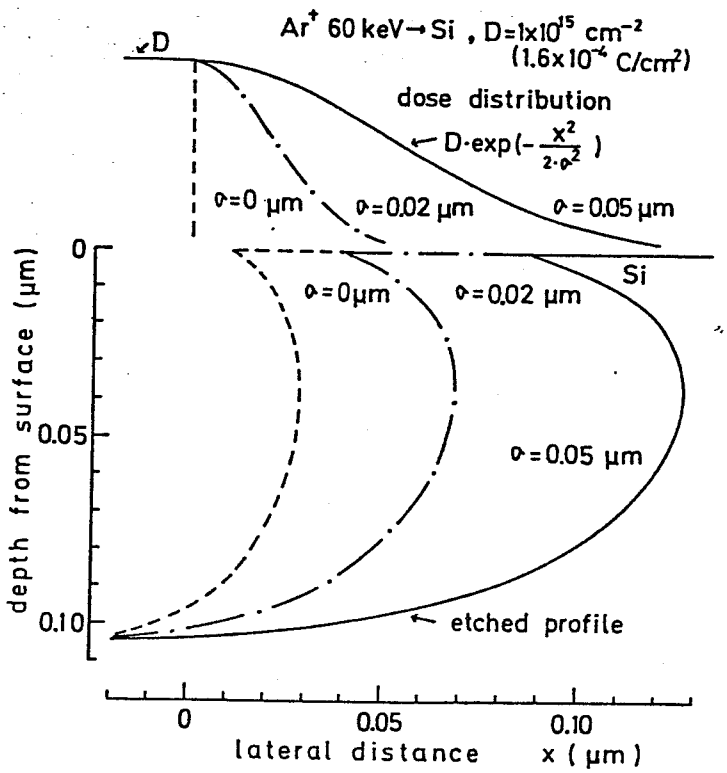

Fig. 3-12. The same calculation as that of Fig. 3-11. Distribution of the incident ion-beam is varied.

3-4-4. Optimum condition

In this section, the optimum dose is to determined for fabricating submicron patterns by investigating side etching and the etched profile.

In Fig. 3-8, as the ion dose increases, the side wall of etched Si becomes vertical and the amount of side etching

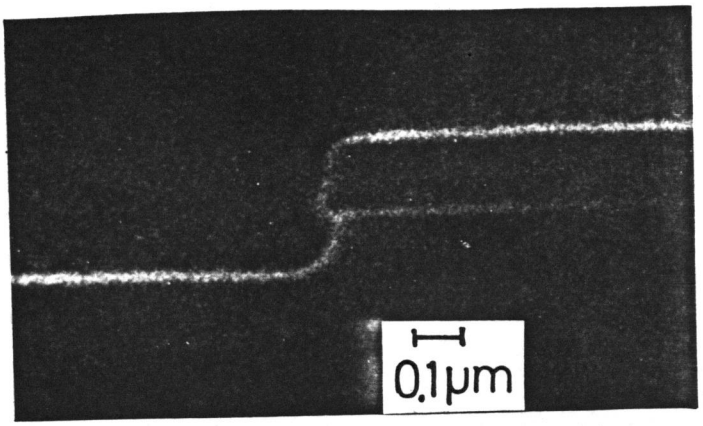

(a) Ar^+ 60 keV , 2×10^{15} cm^{-2}
(3.2×10^{-4} C/cm^2)

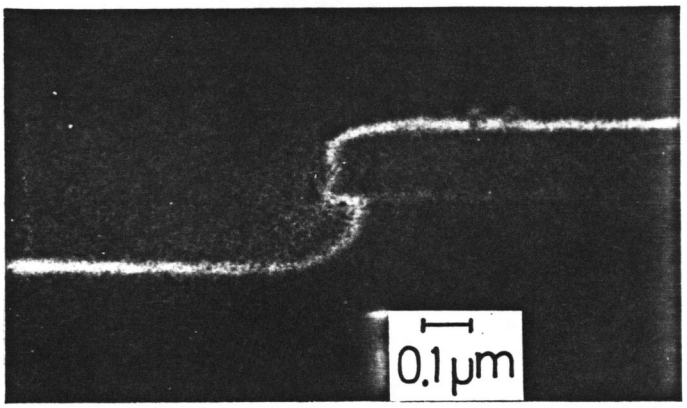

(b) Ar^+ 60 keV , 5×10^{15} cm^{-2}
(8×10^{-4} C/cm^2)

Fig. 3-13. SEM photographs of etched Si profile at a pattern edge together with the Cr mask.

increases. There exists an optimum ion-dose for obtaining a pattern with a small amount of side etching and vertical side wall. Figure 3-13 shows SEM photographs of the etched Si with Cr mask. The amount of side etching was measured from the photographs of Fig. 3-13 and others. Figure 3-14 is a comparison of the amount of calculated side etching with observed side etching. The etched depth normal to the surface is also shown in Fig. 3-14 for comparison. The experimental error of the amount of side etching presented in Fig. 3-14 originates from the resolution of the SEM, as seen in Fig. 3-13. Though the calculated amount of side eching is more than the observed one at relatively low doses, and less at relatively high doses, the

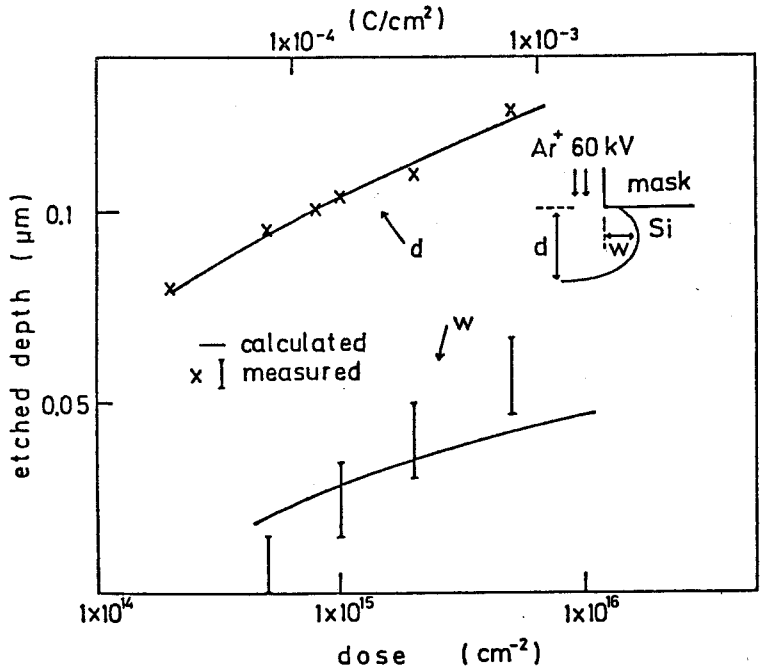

Fig. 3-14. Calculated and measured value of etched depth in both lateral and depth directions by varying ion-dose.

calculated and observed values agree on the whole. The reason for this small discrepancy is not clear.

As the ion dose decreases, the amount of side etching decreases but the curvature of the side wall increases. Figure 3-15 shows the calculated value "a" which represents the bending of the side wall depicted in the figure. The bend in the etched profile becomes extreme at a dose below $1x10^{15}$ Ar/cm^2 in Fig. 3-15. So, at doses of $0.8\text{-}2x10^{15}$ Ar/cm^2, good patterns could be made with sharp edges and with an amount of side etching less than 1/10 of a submicron pattern width.

It was confirmed that a Si pattern with a pattern width of less than 0.1 μm can be fabricated at an ion energy of 60 keV because the amount of side etching is less than 30 nm at a dose below $2x10^{15}$ Ar/cm^2. The resolution is limited by the lateral straggling of incident ions.

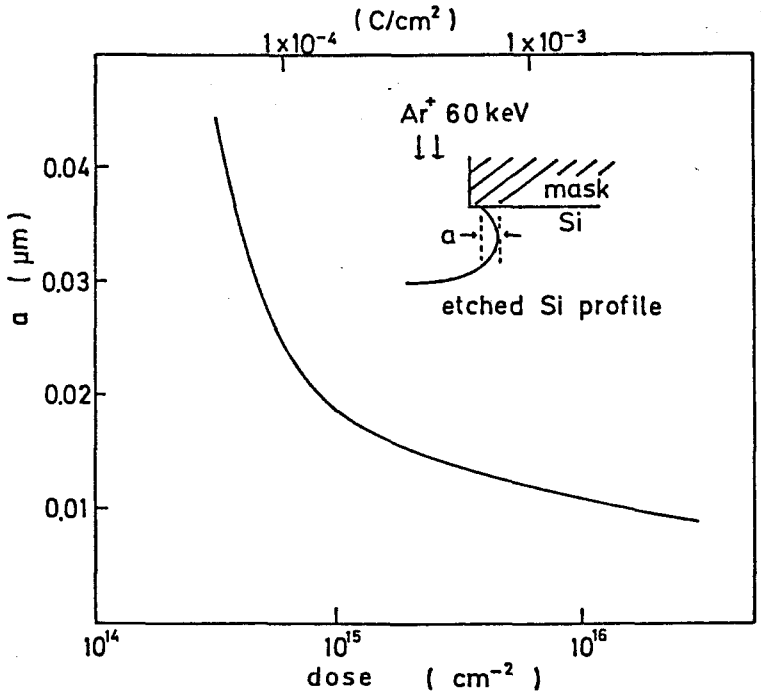

Fig. 3-15. Degree of bending in etched Si profile under pattern mask. Degree of bending is represented by "a" in the figure.

3-4-5. Fabrication of Submicron Pattern

Investigation of the amount of side etching under the mask pattern is very important for confirmation of the high resolution of IBECE. Cr was found to be a suitable mask materials for a procedure such as that in Fig. 3-2 because Cr has a good adhesion to Si substrate and is not etched by diluted HF. A Cr thickness of 0.1 μm was sufficient to stop the 60 keV Ar ions because the sum of Ar ion range and range atraggling of 60 keV Ar in Cr is calculated to be 38.5 nm. Deep etching is possible by repeating this process as shown in Fig. 3-2. Figure 3-16 shows a cross-section of Si line pattern with 1 μm width and 0.21 μm

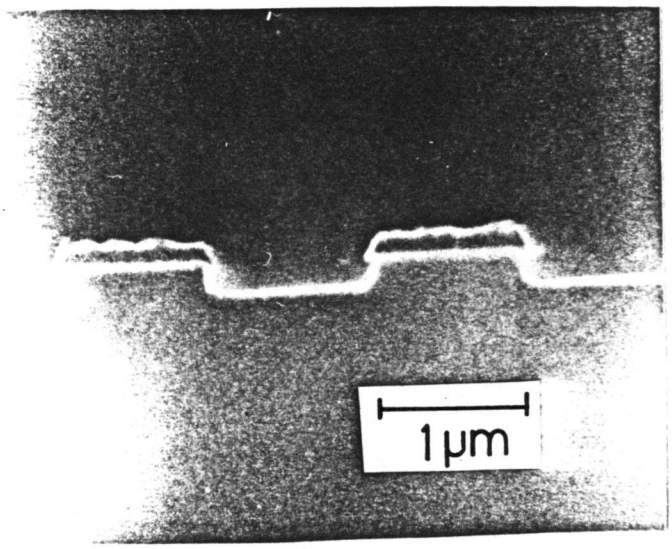

Fig. 3-16. Cross section of Si pattern fabricated by the process shown in Fig. 3-2. Ion bombardment and etching are repeated twice, remaining the Cr mask. Each ion dose is $1 \times 10^{15} C/cm^2$.

thickness fomed by the present procedure. The Cr masks are seen on the top of the Si lines. Ion-bombardment and etching were repeated twice for this sample. The pattern edge is almost vertically walled and the amount of side etching is measured to be 40 nm. As discussed in section 3-4-4, there is an optimum dose for obtaining an exact transfer of mask pattern width to a substrate with an amount of side etching of less than 0.1 m. Above the optimum dose, side etching due to the lateral spread of damage increased greatly. Below the optimum dose, the edge of the Si pattern tapered outside the edge of the Cr mask pattern.

Figure 3-17 shows a cross-section of Si grating pattern after Cr removal with 0.6 m period and 0.25 m line width. This

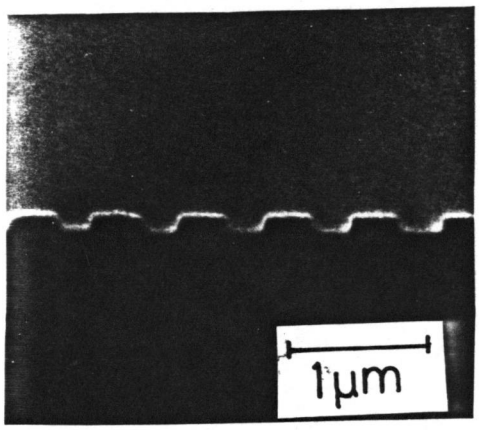

Fig. 3-17. Cross section of Si pattern fabricated by the process shown in Fig. 3-2. The line width is 0.34 μm and the period is 0.6 μm. The ion dose is $1x10^{15}$ Ar/cm^2.

pattern was made by a single ion bombardment. It is verified that a fine pattern with submicron width can be formed in Si substrate by the IBECE technique as shown in Fig. 3-2, and an even finer pattern (0.1 μm) is expected to be fabricated by this technique using a finer Cr mask pattern, judging from the amount of side etching observed. High resolution of IBECE is also confirmed by the photograph in Fig. 3-18. Figure 3-18 shows a comparison of top view of pattern edge between the etched Si and the Cr mask by shifting the mask forcedly using ultrasonic agitator. The edge roughness of Cr with less than 50 nm width was found to be accurately transfered.

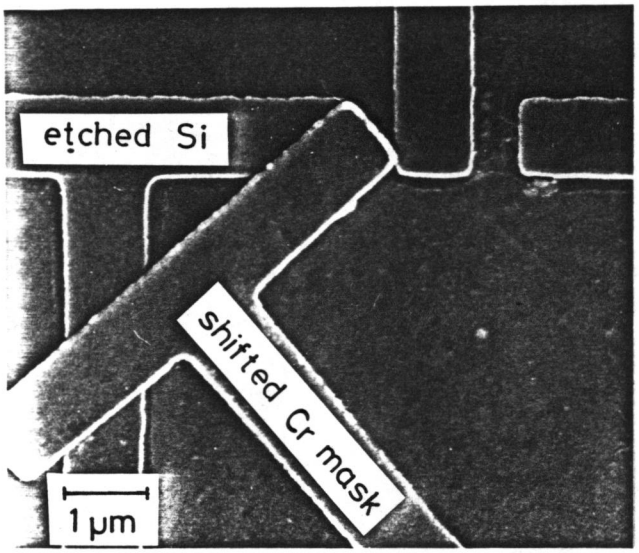

Fig. 3-18. Top view of etched Si and the Cr mask shifted forcedly after the etching to see the accuracy for thr pattern transfer.

3-5. IBECE caracteristics of SiO_2

IBECE effct is not so remarkable for amorphous material like fused quartz as for crystal like Si. As SiO_2 has been widely used for Si LSI or optical elements, high resolution pattern by IBECE OF SiO_2 would be very useful.

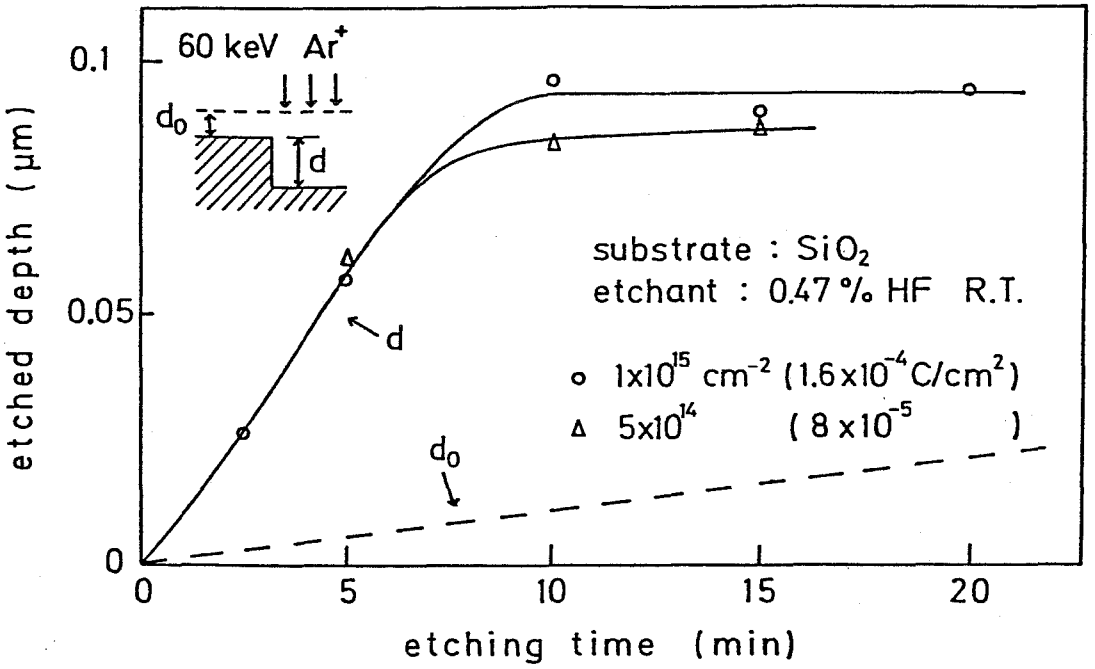

Fig. 3-19. Etched depth of SiO_2 as a function of etching time. The broken line shows the etched depth for unbombarded part of SiO_2.

Figure 3-19 shows characteristics of IBECE for fuzed quartz. The broken line in Fig. 3-19 indicate the etched depth of unbombarded part. The etched depth ratio d/d_0 rises to 8 at its maximum with an ion dose of $5x10^{14}$ Ar/cm^2. It is possible to form patterns in fuzed quartz by IBECE.

Figure 3-20 is a SEM photograph to show top view of grating pattern with 0.6 μm period in fuzed quartz. High resolution property of IBECE was demonstrated for amorphous substrate of fused quartz.

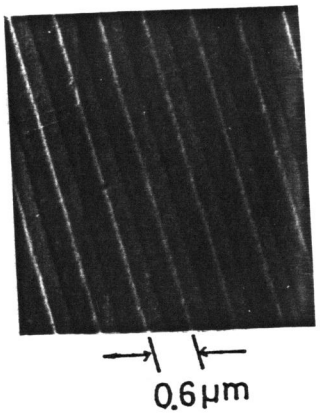

Fig. 3-20. Top view of grating pattern in fused quartz fabricated by the process shown in Fig. 3-2. The ion dose is $5x10^{14}$ Ar/cm^2.

3-6. Conclusions

In this chapter the basic characteristics of the IBECE of Si and SiO_2 are investigated, using 60 keV-Ar as the bombarding ion, with regard to its application to nanmometer lithography.

The etched depth can be controlled from 83 to 128 nm by varying the ion dose with an accuracy of 10 nm, by which the threshould deposited energy defining etched profile was determined to be $4x10^{23}eV/cm^3$.

The etched profile of Si under a mask by IBECE has been investigated. Changes in the etched profile have been studied by varying ion dose at a fixed Ar-ion energy of 60 keV.

The etched profile was calculated by assuming an ideal mask with sufficient thickness and a vertical edge. The experimantally observed profile agreed very well with the calculated one at doses more than $5x10^{15}$ cm^{-2}. With doses smaller than $5x10^{15}$ cm^{-2}, the etched profile at the surface was found to influenced by ions penetrating through the mask edge. Because of this, the bending at the surface of the etched profile is not observed below a dose of $5x10^{15}$ cm^{-2}.

It is concluded that the optimum dose for obtaining submicron patters with sharp edges and a small amount of side etching less than 30 nm is $0.8\text{-}2x10^{15}$ $cm^{-2}$for 60 keV Ar.

The etched profile of Si by maskless lithography with an ion beam of Gaussian distribution is also calculated. In focused-type scanning ion-beam lithography, IBECE will become one

of the most useful technique in the future, as well as being a technique for transferring mask patterns to the substrate.

High resolution of IBECE was demonstrated by fabricating grating patterns with 0.6 μm period in Si and SiO_2.

It sould be pointed out that maskless ion-bombardment and the following dry development of the pattern using reactive plasma for IBECE becomes possible in the future.

References

1) U.F.Giarora:J. Appl. Phys. 28 (1957) 8.

2) D.J.Mazey, R.S.Nelson and R.S.Barnes:Philos. Mag. 17 (1968) 1145.

3) J.F.Gibbons, F.O.Hechfl and T.Tsurushima: Appl. Phys. Lett. 15 (1969) 117.

4) W.A.Johnson, J.C.North and R.Wolfe: J. Appl. Phys. 44 (1973) 4753.

5) M.Kawabe, M,.Kubota, K.Masuda and S, Namba: J. Vac. Sci. Technol. 15 (1978) 1096.

6) T.Tsurushima: Doctor thesis (1978 Osaka University).

7) M.Kawabe, S.Hirata and S.Namba: IEEE Tr. Circuit & Syst. CAS-26 (1979) 1109.

8) V.Wang, J.W.Ward and R.L.Seliger: J. Vac. Sci. Technol. 19 (1981) 1158.

9) K.Moriwaki, N.Masuda, H.Aritome and S.Namba: Jpn. J. Appl. Phys. 19 (1980) 491.

10) K.Moriwaki, H.Aritome and S.Namba: Proc. Micrcircuit Engineering -Microstructure Fabrication- , Sept. 1979 Aachen 153.

11) K.Moriwaki, H.Aritome and S.Namba: Jpn. J. Appl. Phys. 20 (1981) 1305.

12) K.B.Winterbon: Ion Implantation Ranges and Energy Deposition Distribution (IPF/Plenum Press, New York, 1975) vol.2.

13) S.T.Picraux, W.H.Weisenberger and F.L.Vook: Rad. Eff. 7 (1975) 101.

14) F.F.Morehead,Jr. and B.L.Crowder: Rad. Eff. 6 (1970) 27.

15) H.Matsumura and S.Furukawa: J. Appl. Phys. 47 (1976) 1746.

4. Application of Au Free-Standing Mask to X-Ray Transmission-Grating

4-1. Introduction

As discussed previous chapter, Au free-standing mask are very useful for pattern transfer in IBER. In this chapter The Au mask have been shown to be able to apply to the transmission grating,[1-6] which is of great importance for soft x-ray spectroscppy. Because it expected to be the only dispersion element in a wavelength region of 2-5 nm and also expected to be affcted hardly by surface contamination during high-intensity irradiation, which is a severe problem of reflection-type grating for synchrotron radiation spectroscopy.

It is discussed that Au grating can be reproduced by IBER technique accurately.

Calculation of the diffraction efficiency for the grating in soft x-ray wavelength have been performed in the section 4-2. Fabrication process of the grating is described in the section 4-3.

4-2. Calculation of Diffraction Efficiency

In soft x-ray region, we must consider the transmitted wave through the grating bar. Figure 4-1 shows schematic

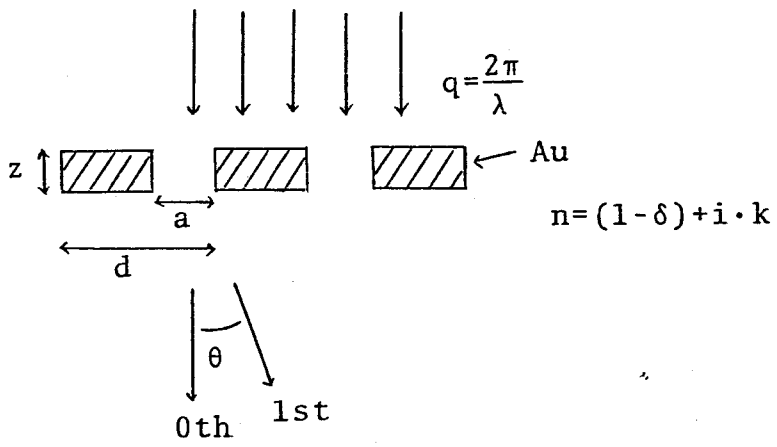

absolute efficiency for m-th order

$$\begin{cases} \eta_m = \left(\frac{\sin(a/d)m\pi}{m\pi}\right)^2 \cdot [\ 1 + \exp(-2qkz) \\ \qquad + 2\cdot(\exp(-qkz))\cdot\cos(q\delta z-(a/d)m\pi)] & (m\neq 0) \\ \eta_{m=0} = (a/d)^2 + (1-(a/d))^2\cdot\exp(-2qkz) \\ \qquad + 2\cdot(a/d)\cdot(1-(a/d))\cdot\exp(-qkz)\cdot\cos(q\delta z) \end{cases}$$

for a/d = 0.5

$$\begin{cases} \eta_{m=odd} = \left(\frac{1}{m\pi}\right)^2 \cdot [\ 1 + \exp(-2qkz) \\ \qquad - 2\cdot\exp(-qkz)\cdot\cos(q\delta z)] \\ \eta_{m=even} = 0 \end{cases}$$

Fig. 4-1. Schematic arrangement of Au transmission grating and equations to calculate diffraction efficiency considering the transmitted wave through the grating bar.

arrangement of transmiossion grating and the equations to calculate the diffraction efficiency, considering transmitted wave through the grating bar, where the nototions are as follows.

q: wave number of the incident radiation

n: complex refractive index of Au

θ: diffraction angle

d: grating period

a: width of open space in the grating

z: thickness of the grating bar

The calculated results are shown in Figs. 4-2, 4-3 and 4-4. The ratio a/d is important for maximum efficiency as shown in Fig. 4-2. It can be seen that the requierd Au thickness of the grating bar is 0.2 μm, in Fig. 4-3.

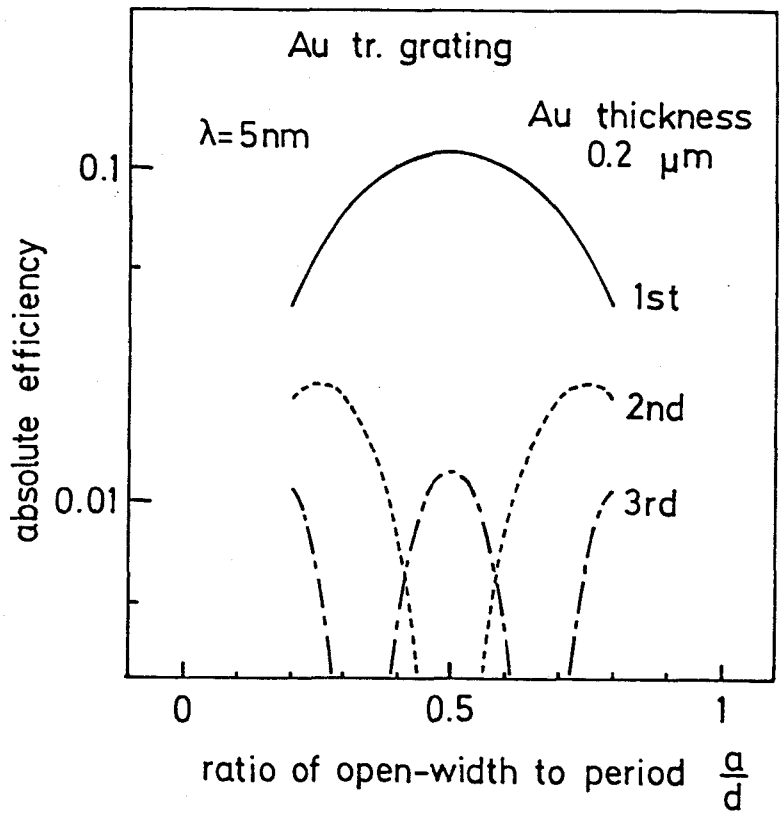

Fig. 4-2. Calculated efficiency as a function of the ratio a/d.

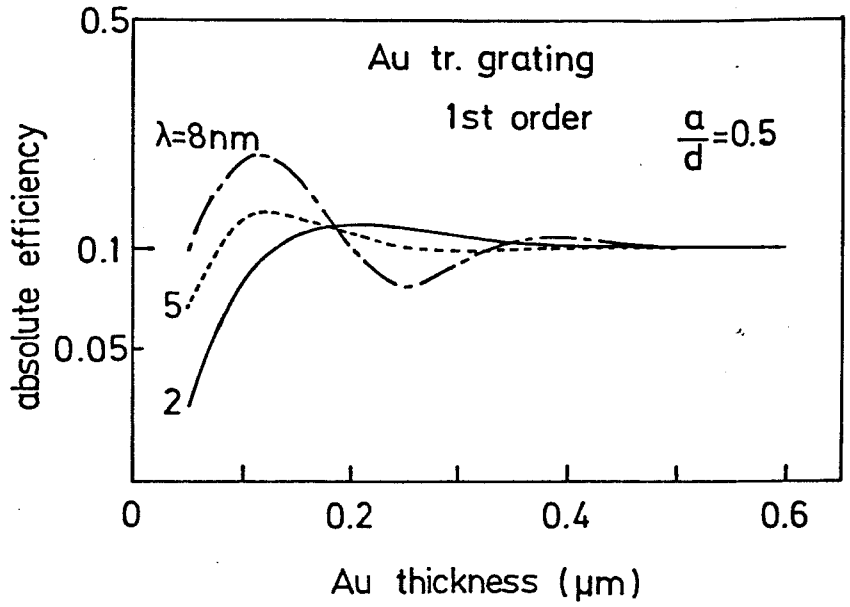

Fig. 4-3. Calculated efficiency as a function of grating Au thickness for a/d=0.5.

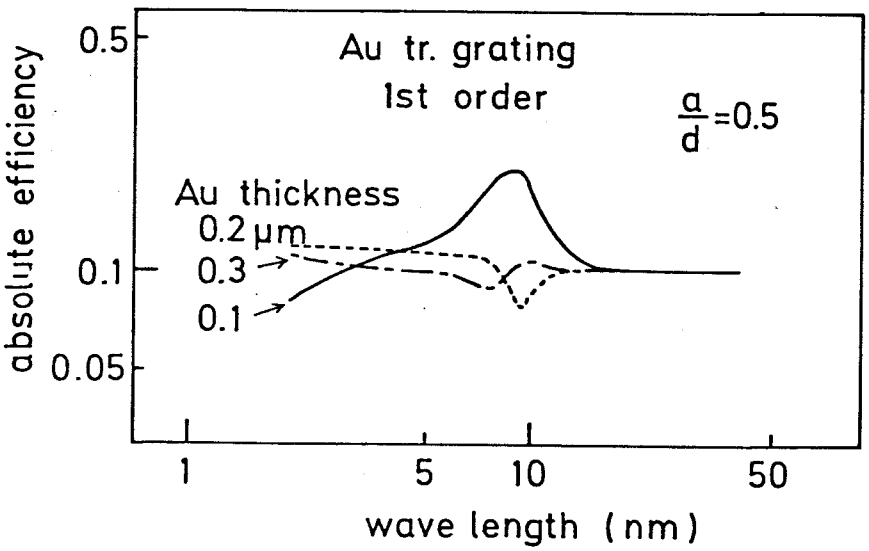

Fig. 4-4. Calculated efficiency as a function of wavelength.

4-3. Fabrication of Au Transmission-Grating

Figure 4-5 shows fabrication process developed in the present work. The original pattern were fabricated by EBL because the ratio of a/d is easily controllable and produce smooth edge of the pattern. The Au pattern were fabricated by electroplating or lift off. Rough grid was used to support the grating bar.

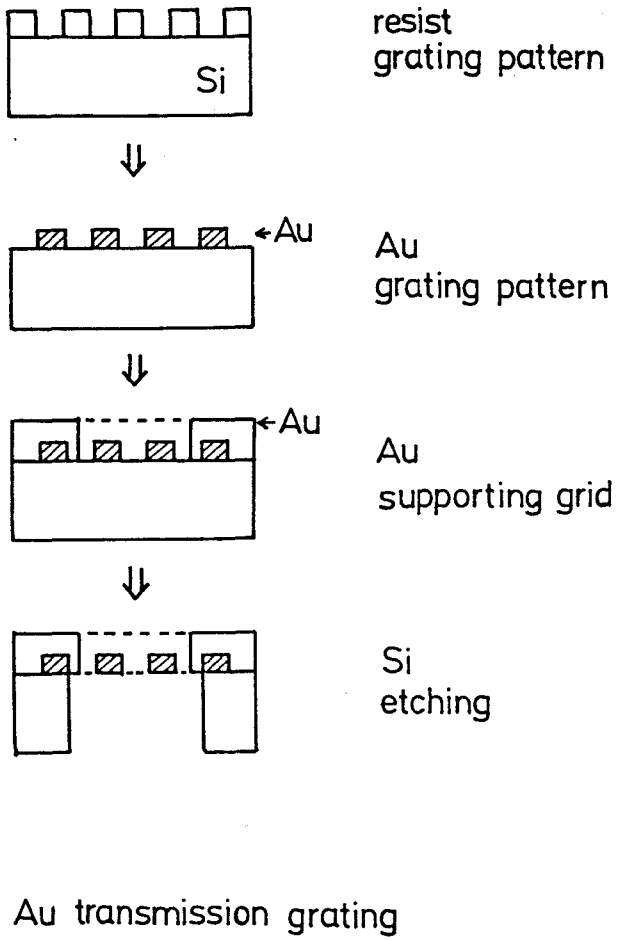

Fig. 4-5. Fabrication process of transmission grating with Si rim.

Figure 4-6 are photographs of a Au transmission grating with a thickness of 0.18 m for two magnifications. The period of the grating is 2 m, and 0.8 m period gratings were fabricated by the present process.

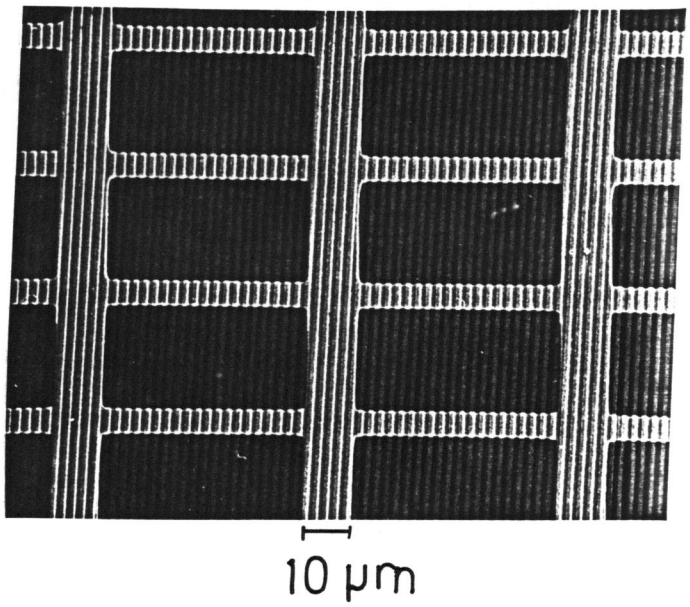

Fig. 4-6. SEM photograph of Au transmission grating

The transmission grating can be reproduced accurately by IBER. Figure 4-7 is a photograph demonstrating replication of PMMA pattern by 50 keV proton beam, as was described in the chapter 2.

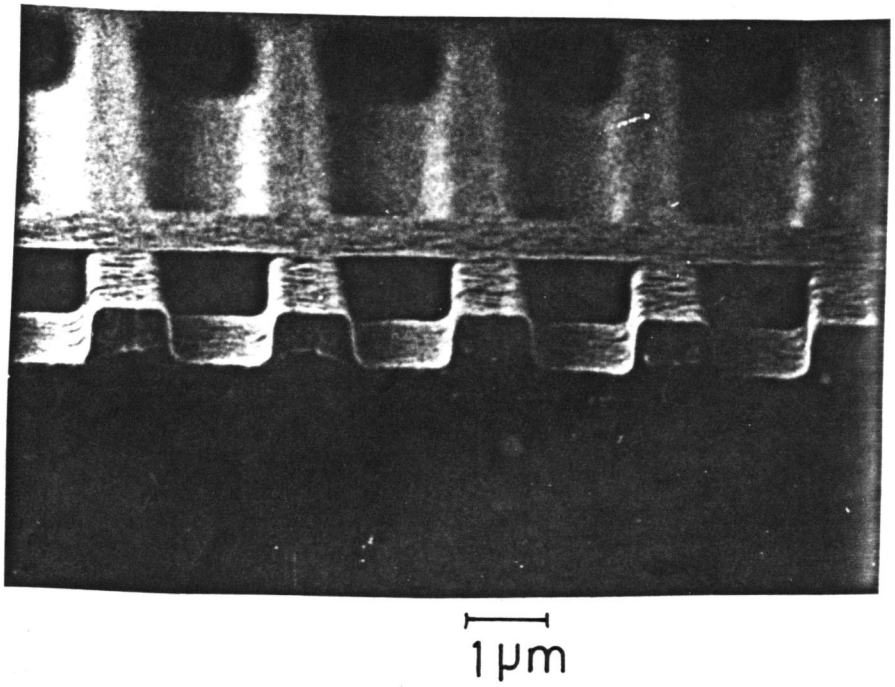

Fig. 4-7. Replicated PMMA pattern of Au transmission grating by IBER.

4-4. Conclusions

In this chapter Au free-standing mask was applied to transmission grating for x-ray spectroscpy.

Successful transmission gratings were fabricated by using EBL and lift off process.

The transmission grating was shown to be reproducible by using IBER technique.

References

1) H.W.Schnopper et al.: Appl. Opt. 16 (1977) 1088.

2) H.Braeuninger, P.Predehl and K.P.Beuermann: Appl. Opt. 18 (1979) 368.

3) H.Braeuninger et al.: Appl. Opt. 18 (1979) 3502.

4) A.C.Brinkman et al.: Appl.Opt. 19 (1980) 287.

5) R.Tachyn and I.Lindau: Nuclear Instrum. Methods 172 (1980) 287.

6) A.M.Hawryluk, N.M.Seglio, R.H.Price, J.Melngailis and H.I.Smith: J. Vac. Sci. Technol. 19 (1981) 897.

7) H.J.Hagemann, W.Gudat and C.Kunz: J. Opt. Soc. Am. 65 (1975) 742.

5. Conclusions

Ion-beam lithography for fabricating devices with nanomater structures has been studied.

IBER have been investigated using 50 keV proton beam and PMMA, FPM and AZ1350 resists.

Sensitivity for IBER was found to be higher than that for EBL by about two order of magnitude.

As for PMMA, the developed thickness after proton beam exposure were studied in detail. Simple process for calculating the developed thickness was developed and the results were in good agreement with experiments. And the projected ion range and the standard deviation of the range was determined to be 650 nm and 30 nm, respectively.

Au free-standing mask were fabricated to demonstrate the high resolution of IBER. Fine structure (50 nm width) at the edge of the mask pattern was replicated in PMMA

80 nm wide FPM pattern was fabricated with a low dose of $3x10^{-7}$ C/cm^2 by IBER, which show the high resolution of the IBER technique itself rather than that of resist. Together with successful fabrication of 300 nm wide pattern of AZ1350, it is verified that various resist canbe used in nonometer region by using IBER.

IBECE of Si and SiO have been studied using 60 keV Ar beam

for nanometer lithography.

The etched depth of Si was controlled with 10 nm accuracy by varying the ion dose from 83 to 128 nm, which was predicted by calculating the deposited enegy in Si assuming the threshold enegy of $4x10^{23}eV/cm^2$.

The etched profile of Si is investigated to demonstrate high resolution of IBECE. It is concluded by calculation and experiment that the undercuttig of the pattern can be less than 30 nm, so 0.1 μm pattern can be possible.

Optimum dose to fabricate fine line with sharp edge was found to be $0.8\text{-}2x10^{15}cm^{-2}$ for 60 keV Ar.

The Au free-standing mask have been apllied to x-ray transmission grating. Successful grating was fabricated using EBL and was shown to be reproducible by IBER.

Acknowledgement

This work has been performed at Faculty of Engineering Science of Osaka University, Toyonaka, Osaka, under Professor Namba's guidance.

The author would like to express his sincere thanks to Prof. Namba for his continuous guidance and encouragement.

The author would like to thank to Professors Fujisawa, Sueta, Hamakawa and Yamamoto for their guidance in Osaka University.

Much appreciation to Professos H.Aritome and K.Gamo should be expressed for their continuous and kind discussions.

The author would like to thank to all of the member in Namba laboatory particularly to Drs S.Matsui, M.Takai, Y.Yuba. and Messrs. K.Mino, K.Kawasaki, M.Nishida, N.Masuda, Yamato amd other students for thier experimental support and discussions

Some of the work on IBER of FPM resist was carried out in the NRRFSS of Cornell Univ. USA, The author would like to thank the staff of the NRRFSS particularly to Professors E.D.Wolf and C.A.Lee and Drs. L.Farapiperis, I.Adesida and N.J.Kawai, for their kind help and support.

The staffs of the Institute of Solid State Physics, Tokyo University are also much appreciated for their useful discussions.